ISSN 0869-5911, Petrology, 2015, Vol. 23, No. 6, pp. 519–542. © Pleiades Publishing, Ltd., 2015.
Original Russian Text © I.P. Solovova, L.N. Kogarko, A.A. Averin, 2015, published in Petrologiya, 2015, Vol. 23, No. 6, pp. 563–588.

Conditions of Sulfide Formation in the Metasomatized Mantle beneath East Antarctica

I. P. Solovova[a], L. N. Kogarko[b], and A. A. Averin[c]

[a] *Institute of Geology of Ore Deposits, Petrography, Mineralogy, and Geochemistry (IGEM), Russian Academy of Sciences, Staromonetnyi per. 35, Moscow, 119017 Russia*

e-mail: solovova@igem.ru

[b] *Vernadsky Institute of Geochemistry and Analytical Chemistry, Russian Academy of Sciences, ul. Kosygina 19, Moscow, 119991 Russia*

[c] *Frumkin Institute of Physical Chemistry and Electrochemistry, Leninskii pr. 31, Moscow, 119071 Russia*

Received May 16, 2015; in final form, June 29, 2015

Abstract—Garnet–spinel lherzolites from Antarctica and peridotites from Mongolia were fluid saturated, which is indicated by the presence of fluid inclusions in their minerals. Flows of reactive fluids caused extensive metasomatic alteration of mantle materials. The cryometric and Raman spectroscopic investigation of the Antarctic xenoliths showed that their fluid was a complex mixture of CO_2, N_2, H_2S, and H_2O with a density of up to 1.23 g/cm^3. The entrapment of fluids was accompanied by the formation of clusters of numerous sulfide inclusions. The compositions of these inclusions correspond to a Ni-rich sulfide melt and a monosulfide solid solution. The partition coefficient of Ni between them (D_{Ni} *mss*/melt) ranges from 0.99 to 3.23, which suggests that the two-phase sulfide assemblages in the partly decrepitated inclusions equilibrated at 920–1060°C. In order to refine the initial *P-T* conditions of the development of the Antarctic peridotites, the results of our investigation were evaluated in the light of experimental data on (1) the stability field of the two-phase assemblage *mss* + sulfide melt, (2) the solidus of peridotite + $0.9CO_2$ + 0.1 H_2O, and (3) isochores of $0.8CO_2$ + $0.2N_2$ fluid. The obtained parameters are close to 1270–1280°C and 2.2 GPa and lie near the *Sp–Gar* boundary. The temperature of the existence of *sulfide melt* at a pressure of 2.2 GPa must be near 1300°C and corresponds to the boundary between the occurrence of carbon as CO_2 fluid and carbonate (carbonate melt).

DOI: 10.1134/S0869591115060053

INTRODUCTION

Mantle xenoliths in kimberlites and alkaline mafic–ultramafic volcanic rocks provide important information on processes in the deep levels of the Earth. Their investigation demonstrated that a free fluid phase could occur in the mantle; and the finding of sulfides, which are the main hosts for transition and precious metals, such as Ni, Cu, Pt, Pd, and Au, implies high S concentrations (Lorand, 1990). The mantle is considered by many authors as the main source of matter for magmatic sulfide deposits. It was supposed that wide variations in the chemical and mineral compositions of magmatic sulfide deposits are the consequence of either fractional crystallization of initial sulfide melts (Naldrett et al., 1997) or leaching and subsequent redeposition under the influence of fluids (Farrow and Watkinson, 1992). Krivolutskaya (2014) hypothesized on the basis of the investigation of S isotope systematics that mantle magmas could be not only S sources but also sulfide transporting agents.

The investigation of microinclusions in minerals may shed light on the nature and composition of fluid phase in the mantle and the evolution of volatile components and primary sulfides under varying physicochemical parameters. The investigation of inclusions demonstrated the possibility of coexistence of three immiscible mobile phases of contrasting composition, sulfide, silicate, and fluid, in the mantle (Kovalenko et al., 1986).

The overwhelming majority of studies of fluid inclusions in mantle minerals established the dominance of CO_2 in their composition. Ryabchikov (1985) showed that the identity and proportions of compounds in the C–H–O system depend on redox conditions: CO_2 and H_2O are dominant at a high redox potential, whereas, under reducing conditions, mantle fluid must contain hydrocarbons (primarily, CH_4) with the appearance of graphite or, at high pressure, diamond. Note that inclusions containing significant amounts of H_2O are rare, which is explained by high H_2O solubility in partial silicate melts and crystallization of hydrous minerals (mica, amphibole, etc.).

The main target of our study was garnet–spinel lherzolites affected by extensive carbonate metasomatism from East Antarctica. We present compelling evidence for the presence of multicomponent (CO_2, N_2, H_2S, and H_2O) fluids coexisting with sulfide liquid and silicate magma in the upper mantle.

Despite numerous studies, the state of sulfide material at great depths is still a topic of considerable interest. Its identification as sulfide melt or monosulfide solid solution (*mss*) is usually based on experimentally determined phase equilibria and partition coefficients of platinum group elements and, recently, also Se and Te between them (Brenan, 2015). The most popular criteria for determining the phase state of sulfide material are the droplike shape of inclusions and haloes of tiny satellite inclusions around them (attributed to partial decrepitation) as indirect evidence for their initially liquid state. Our data in comparison with available experimental evidence confirmed this suggestion in fact for the first time.

For comparison, this paper presents also the characteristics of fluid and fluid–sulfide–silicate inclusions in the minerals of a mantle garnet–pyroxene druse and vesicular clinopyroxene megacrysts from Shavaryn-Tsaram (Mongolia).

METHODS

Doubly polished wafers up to 0.3 mm thick were prepared for the investigation of inclusions in minerals. Fluid inclusions were examined optically using a Linkam THMSG 600 heating–freezing stage cooled with liquid nitrogen (to −180°C). The stage was calibrated using synthetic fluid inclusions of CO_2 and salt solutions of known concentration. The temperature and cooling rate conditions of cryometric experiments were maintained using a programmed controller.

Solid phases were analyzed using a JXA-8100 JEOL electron microprobe (analyst I.G. Griboedova, IGEM RAS). Analyses were made at 15 or 30 kV accelerating voltage, 20 or 30 nA beam current, and an electron beam diameter of 1, 2, or 5 μm. Certified natural minerals and glasses were used as standards: USNM 111240/2 (basalt glass VG-2) for Si, Al, Fe, Mg, and Ca; jadeite for Na; orthoclase for K; rhodonite for Mn; TiO_2 for Ti; ZrO_2 for Zr; MgF_2 for F; vanadinite for Cl; $CuFeS_2$ for Cu, Fe, and S; and Ni metal for Ni. Sulfide inclusions were also analyzed using a JSM-5610LV (Japan) scanning electron microscope (analyst L.O. Magazina, IGEM RAS) equipped with an energy dispersive analytical spectrometer JED-2300 (Japan). The analytical conditions were as follows: a beam diameter of 1 μm, an accelerating voltage of 25 kV, and a takeoff angle of 45°. The detection limit for elements with middle atomic masses was ~0.1%.

The Raman spectra of phases and inclusions were recorder using a Bruker SENTERRA spectrometer at the Frumkin Institute of Physical Chemistry and Electrochemistry of the Russian Academy of Sciences. The registration parameters were as follows: a laser wavelength of 532 nm (λ), a power of 2–10 mW depending on the sample, a spectral resolution of ~3 cm^{-1}, a 20–50× objective, and a spectrum acquisition time of 500 s.

SHORT PETROGRAPHIC AND MINERALOGICAL DESCRIPTION OF XENOLITHS

Diatreme and dike bodies with xenoliths were investigated in the Jetty Oasis in the eastern zone of the Beaver Lake rift system, Prince Charles Mountains (East Antarctica). They are made up of alkaline ultrabasic rocks, including alkaline olivine–pyroxene picrites, nepheline–melilite–pyroxene picrites, olivine melanephelinites, and lamprophyres (Mikhalsky et al., 1998). The K–Ar age of the bodies is 113–150 Ma (Laiba et al., 1987). The recent data of Belyatsky and Andronikov (2009) further constrained the age to lie within 105–129 Ma. The alkaline picrites contain up to 39 wt % SiO_2, 19.5 wt % MgO, and 3.4 wt % total alkalis at $Na_2O/K_2O = 0.87$ and Al_2O_3 content up to 6 wt %. High loss on ignition values (up to 11%) are related to the presence of significant amounts of secondary hydrous minerals (Mikhalsky et al., 1998).

The mantle xenoliths are garnet–spinel and spinel lherzolites, dunites, harzburgites, and wehrlites (Andronikov and Mikhalsky, 1997) and account for up to 30% of the rock volume (Foley et al., 2006). Approximately 90% of xenoliths from the southern body are garnet–spinel peridotites. We investigated two samples of coarse-grained sheared garnet–spinel lherzolites up to 50 cm in size. They show high MgO contents (up to 42 wt %), $Fe^{3+}/Fe^{2+} = 0.32$, and relatively high loss on ignition values (4.4 wt % at a standard deviation of 2.2 wt %) (Belyatsky and Andronikov, 2009).

The major minerals of the xenoliths are olivine, orthopyroxene, clinopyroxene, spinel, and garnet; their compositions were described in detail by Foley et al. (2006). The phases show complex morphological relationships suggesting the extensive metasomatic reworking of the peridotite and the prolonged history of the development of its observed features. Four stages of alteration of mantle material accompanied by periodic changes in *P-T* conditions were distinguished. The multistage evolution is confirmed by petrographic examination. Transparent and euhedral olivine and orthopyroxene grains coexist with deformed, turbid, and fractured crystals. Spinel grains often have resorbed margins and a fine-grained texture. They are rich in Al_2O_3 (up to 53 wt %), NiO (up to 0.36 wt %), and Cr_2O_3 (up to 14.6 wt %, and even up to 21 wt % according to Foley et al., 2006). Olivine and orthopyroxene host crystalline inclusions of clinopyroxene, spinel, garnet, and olivine of spherical shape up to 150 μm across. The grains of rock-forming olivine and olivine inclusions show similar *mg#* values (up to 0.91) and contents of CaO (~0.11 wt %) and NiO (up to 0.50 wt %). The garnet composition is dominated by the pyrope component. Its large (up to centimeter-sized) grains are replaced partly or completely by a very fine-grained aggregate (kelyphite material), which formed around garnet grains in the zone of its

thermodynamic instability and/or during its interaction with fluids or melts (Morishita et al., 2001). Aluminous spinel (up to 63 wt % Al_2O_3, 6 wt % Cr_2O_3, and 0.05 wt % NiO) and a finely crystallized orthopyroxene–clinopyroxene mixture were identified in this aggregate.

The margins of clinopyroxene are resorbed and intersected by sinuous glass (melt) embayments. These zones contain melt inclusions with homogenization temperatures of 970–1000°C. The aluminous calc-alkaline melt of the inclusions contains, on average, 54 wt % SiO_2, up to 11 wt % CaO, and 5 wt % Na_2O. Glass patches up to 150–200 μm across occur also in the intergranular space. It embeds newly formed clinopyroxene, late-generation olivine and spinel, Ba- and Ti-bearing phlogopite, S-bearing chlorapatite, henrymeyerite, calcite, and dolomite (Kogarko et al., 2007). Carbonates also form veinlet-like aggregates cutting mantle material. Foley et al. (2006) described rare small carbonate inclusions in rock-forming olivine and orthopyroxene.

We investigated also a fragment of a mantle garnet–pyroxenite druse from the pyroclastic rock of the Shavaryn-Tsaram massif, Mongolia (Kovalenko et al., 1986). The sample shows a zoned structure with spinel lherzolite changed by websterite; large crystals and intergrowths of clinopyroxene and garnet (up to 1.5 cm in size) occur on the websterite substrate and are separated by voids and fine-grained clinopyroxene–phlogopite aggregate. The clinopyroxene and garnet are rich in iron and titanium. The clinopyroxene hosts orthopyroxene and phlogopite inclusions with *mg*# values of 0.80 and 0.73, respectively.

Clinopyroxene megacrysts from the Shavaryn-Tsaram massif (*mg*# = 0.74, up to 9.5 wt % Al_2O_3, and up to 1.45 wt % TiO_2) also contain copious voids accounting for up to 10–30% of the pyroxene volume (Kovalenko et al., 1985) and often host pink garnet inclusions up to 5 mm in size.

DESCRIPTION OF INCLUSIONS

Microinclusions of different types—melt, fluid, sulfide, and their combined fluid–sulfide–silicate–(±carbonate) varieties—were observed in the major minerals of the mantle nodules. The inclusions are from 2 to 30 μm in size. The inclusions are surrounded by haloes formed by the part of material lost from the inclusions when they were cracked (partly decrepitated) owing to decompression during xenolith ascent to the surface together with the main volume of their host magmas. The haloes are composed of tiny (no more than 1.5 μm in diameter) satellite inclusions around larger inclusions along radial cracks not extending outside the host mineral (Fig. 1a).

Since the primary inclusions in minerals were isolated from the external medium, we believe that all phase changes in them occurred without input or output of foreign material.

Sulfide Inclusions

Sulfide inclusions of different morphology, phase composition, and chemical characteristics were found in orthopyroxene and olivine from the Antarctica xenoliths and clinopyroxene and garnet from the vesicular mantle megacrysts and druse from Mongolia. The total volume of sulfide phases is up to a few percent in the Mongolian peridotites and no more than a few tenths of percent in the Antarctic xenoliths.

Sulfides inclusions in olivine and orthopyroxene from the Antarctic xenoliths are droplike or oval-shaped and from 2 to 15 μm (usually 5–10 μm) in size. They arrange into clusters of up to 15 (sometimes, more) inclusions within crystals. Partly faceted inclusions and intergrowths of sulfides with silicates and carbonates were occasionally observed by us and mentioned by Foley et al. (2006).

There are also two-phase sulfide inclusions in which one partly faceted phase is embedded in an anhedral matrix. Their relationships are illustrated by a back-scattering electron (BSE) image in Fig. 1b.

Sulfide inclusions in the nodules and megacrysts of the Shavaryn-Tsaram massif in Mongolia show a complex texture typical of liquid immiscibility (Fig. 1c). They are composed of droplike sulfides up to 10 μm in diameter and products of melt crystallization composed of silicate and oxide grains. Residual glass was observed along margins and in the interstitial space. Cavities formed during the opening of thin sections and fluid escape can be seen on the polished surface. Relatively small cavities retain their initial shape, whereas larger vacuoles show evidence for explosion with the formation of large fractures. The proportion of phases is variable, and the silicate constituent sometimes forms only a narrow fringe around a central sulfide grain.

Multiphase inclusions in clinopyroxene and garnet of the Mongolian mantle druse are spherical or oval-shaped and often overprinted by secondary processes related to the development of late fracture systems.

Fluid Inclusions

Primary single-phase (liquid) fluid inclusions with negative crystal shapes and no more than 12 μm in size (Fig. 2a) were found in olivine and orthopyroxene from the Antarctic xenoliths. They coexist with sulfide and multiphase fluid–silicate inclusions, which are composed of partly or completely crystallized melt and two fluid phases, liquid and gas (Fig. 2b). Short cracks cutting across the inclusions do not extend outside the host mineral, which indicates their formation after the conservation of the primary inclusions.

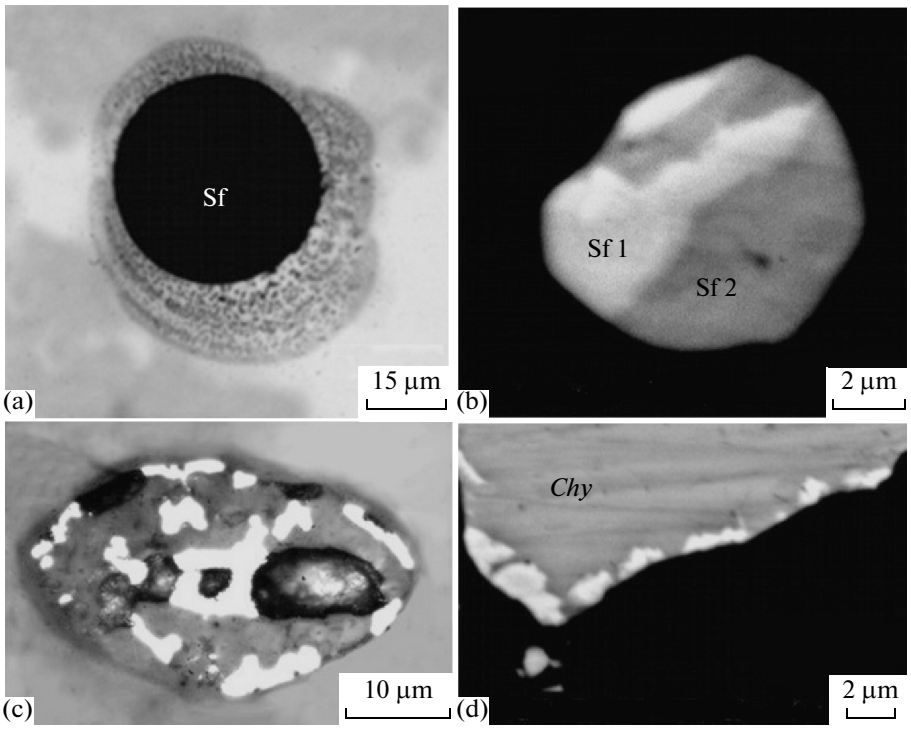

Fig. 1. Images of sulfide inclusions. (a) Transmitted-light photomicrograph of a partly decrepitated sulfide inclusion showing evidence for material loss. (b) Back-scattered electron image of a two-phase sulfide inclusion. (c) Reflected-light photomicrograph of a sulfide–silicate–fluid inclusion with a typical liquid immiscibility texture. White phases are sulfides, light gray phases are silicate minerals (including clinopyroxene), small areas of dark gray color are glass, and black areas are opened fluid cavities. (d) Back-scattered electron image of secondary sulfide grains along the margin of a chalcopyrite crystal. Sf is sulfide, Sf 1 and Sf 2 are two sulfide phases in an inclusion, and *Chy* is chalcopyrite.

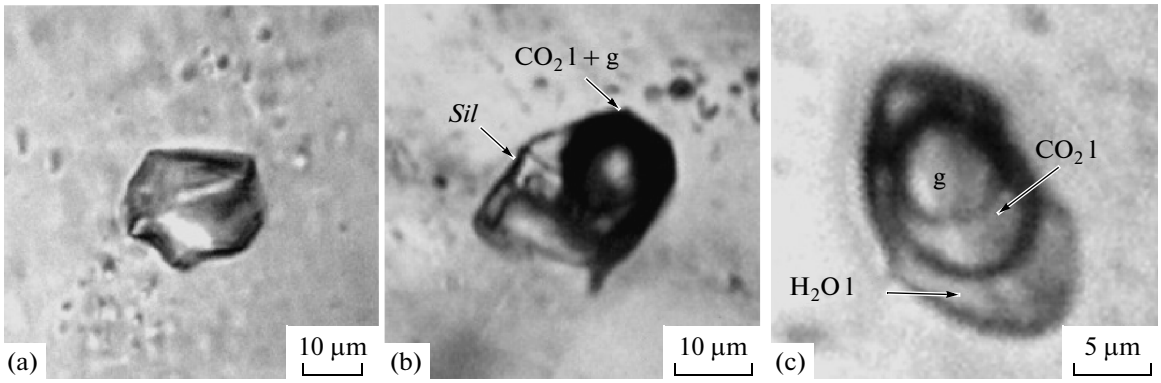

Fig. 2. Photomicrographs of fluid inclusions in the Antarctic xenoliths. (a) Primary high-density fluid inclusions (liquid at room temperature). (b) Combined melt–fluid inclusion in orthopyroxene comprising daughter crystals, glass, and two fluid phases (liquid and gas). (c) Three-phase fluid inclusion with two liquids (H_2O and CO_2) and a gas bubble. *Sil* is the silicate phase of the combined inclusion, g is gas, and l is liquid.

In addition to the primary inclusions, the minerals contain pseudosecondary and secondary fluid inclusions. Because of the strong fracturing of the sample, the decrepitated pseudosecondary and definitely secondary inclusions confined to fractures might be difficult to discriminate. In most cases, they contain two phases, gas and liquid. Rare three-phase gas-bearing inclusions contain carbonate crystals and/or two liquids (CO_2 and H_2O) (Fig. 2c). The partial decrepitation of inclusions may result in coexistence of inclusions with different densities in the same zones of the host mineral. Such inclusions were described in detail by Buikin et al. (2014).

Table 1. Composition of pentlandite from intergranular aggregates, East Antarctica

Component	1*	2	3	4	5	6	7	8	9	10	11
S, wt %	33.13	33.03	33.19	33.08	33.15	33.24	33.79	33.28	33.52	33.57	33.35
Ni	38.86	39.85	40.13	38.94	38.67	39.44	38.22	37.61	39.64	41.69	40.84
Co	0.47	0.43	0.44	0.44	0.49	0.45	0.34	0.44	0.41	0.43	0.35
Fe	27.68	26.74	25.18	27.36	27.49	26.86	26.61	28.42	26.49	24.53	25.25
Cu	0.02	0.00	0.61	0.01	0.04	0.12	0.00	0.02	0.03	0.07	0.10
Total	100.30	100.21	99.74	99.89	100.24	100.14	98.97	99.77	100.08	100.28	99.88
S, at %	46.99	46.93	47.34	47.05	47.13	47.14	48.19	47.28	47.47	47.48	47.38
Ni	30.10	30.92	31.27	30.26	30.03	30.55	29.77	29.19	30.66	32.21	31.69
Co	0.36	0.33	0.34	0.34	0.38	0.35	0.27	0.34	0.32	0.33	0.27
Fe	22.53	21.81	20.62	22.34	22.44	21.87	21.78	23.18	21.53	19.92	20.59
Cu	0.01	0.00	0.44	0.01	0.03	0.08	0.00	0.01	0.02	0.05	0.07
M/S atomic ratio	1.13	1.13	1.11	1.13	1.12	1.12	1.08	1.12	1.11	1.11	1.11
Ni/Fe	1.34	1.42	1.52	1.35	1.34	1.40	1.37	1.26	1.42	1.62	1.54

* Analysis number.

This study focused on the coexisting primary high-density fluid and sulfide inclusions in the minerals of the Antarctic xenoliths.

Clinopyroxenes from the Mongolian xenoliths also contain rare fluid inclusions cogenetic with sulfide and sulfide–silicate–fluid inclusions (Kovalenko et al., 1986). They are tubular in shape and are characterized by decrepitation and partial loss of their material.

INVESTIGATION OF SULFIDE PHASES

The chemistry of magmatic and mantle sulfides is dominated by four major components: S, Fe, Ni, and Cu. The review of published experimental studies (Girnis, 2003) on Ni-bearing sulfide systems suggests that the metal/sulfur ratio (M/S) is one of the most important characteristics of sulfides. The M/S ratio of the majority of experimental sulfides (277 of 283 analyses) ranges from 0.91 to 1.77 at temperatures from 800 to 2200°C and pressures from 0.2 to 50 GPa.

The compositions of sulfide inclusions in minerals and phases from intergranular aggregates are given in Tables 1–3 and plotted in Fig. 3 in the Fe–Ni–S coordinates (Kullerud et al., 1969). The inclusions in the Antarctic xenoliths are enriched in Ni compared with sulfides from Mongolia and S compared with the mean composition of sulfides in mantle peridotites worldwide (Alard et al., 2000). Ryabchikov (2003) noted that elevated Ni contents can be considered as a criterion for the potential platinum enrichment of magmatic melt. It was found that sulfides from the mantle xenoliths of West Antarctica are Fe-rich and correspond to pyrrhotite with a minor Ni admixture (Martin et al., 2014). The Co contents of the sulfides of Antarctica and Mongolia are within 0.11–0.77 wt %.

Sulfide aggregates up to 250 μm in size were observed in the intergranular space of the Antarctic xenoliths. They consist of several sulfide phases, spinel, and secondary products of sulfide alteration. The aggregates are usually irregularly shaped, but spherical segregations were occasionally found (Fig. 4, inset).

Sulfides of Intergranular Aggregates from Antarctica

The sulfides of the multiphase aggregates are pentlandite, chalcopyrite, and minor ternary solid solution (*xss*), the stability of which was experimentally constrained to temperatures below 850°C (Fleet and Pan, 1994). Compared with the intermediate solid solution (*iss*), *xss* is enriched in Ni.

Pentlandite (Table 1) is the most voluminous phase of intergrowths and has an M/S atomic ratio

Table 2. Composition of chalcopyrite from intergranular aggregates, East Antarctica

Component	1*	2	3	4	5	6	7	8	9
S, wt %	35.57	35.17	35.15	34.93	35.26	34.61	34.85	35.38	34.91
Ni	0.52	0.42	3.77	0.57	0.26	0.72	0.57	0.54	0.26
Co	0.06	0.03	0.16	0.07	0.03	0.03	0.04	0.06	0.03
Fe	30.31	30.82	29.53	30.09	29.88	30.40	30.14	30.10	30.42
Cu	33.04	34.08	31.26	33.46	33.93	33.78	33.59	33.18	33.27
Total	99.56	100.63	99.95	99.11	99.35	99.53	99.19	99.26	98.89
S, at %	50.85	50.03	50.20	50.31	50.60	49.79	50.19	50.75	50.36
Ni	0.41	0.32	2.94	0.45	0.20	0.56	0.45	0.42	0.21
Co	0.05	0.03	0.12	0.05	0.02	0.03	0.03	0.04	0.02
Fe	24.87	25.16	24.21	24.88	24.61	25.10	24.91	24.78	25.19
Cu	23.83	24.46	22.53	24.32	24.56	24.52	24.41	24.01	24.22
M/S atomic ratio	0.97	1.00	0.99	0.99	0.98	1.01	0.99	0.97	0.99
Ni/Fe	1.04	1.03	1.07	1.02	1.00	1.02	1.02	1.03	1.04

* Analysis number.

Table 3. Characteristics of the Raman peaks of pentlandite and chalcopyrite

Analysis no.	*Pn*			*Chy*		
	peak	rel. int.	width	peak	rel. int.	width
1	–	–	–	686.4	513.7	107.4
2	663.2	67.4	71.8	–	–	–
3	368.6	396.8	63.6	–	–	–
4	341.0	30.3	15.0	349.5	188.3	21.5
5	–	–	–	317.3	128.6	14.4
6	284.0	246.0	19.1	288.0	2603.0	31.9
7	215.7	28.2	19.9	214.6	119.3	14.6
8	144.6	130.8	18.6	142.8	124.7	37.3

"Peak" is the position of the peak in the spectrum, cm^{-1}; "rel. int." is the relative intensity of the peak; and "width" is the peak width, cm^{-1}.

approaching the stoichiometric value or slightly lower (1.14–1.11). A lower M/S value of 1.08 was observed in a single case. The proportions of Ni and Fe are variable, and Ni always dominates (Ni/Fe from 1.26 to 1.62). Considerable Ni/Fe variations were sometimes observed within a single grain, which indicates its chemical heterogeneity. The mean Cu content is 0.3 at %.

Chalcopyrite occurs at the margins of droplike aggregates (Fig. 4, inset). Its M/S value lies within 1.0–1.07 (Table 2), which almost perfectly matches the formula $CuFeS_2$. The Ni content is 0.20–0.56 at %, and one grain contains 2.94 at % Ni (Table 2, analysis 3).

Figure 4 shows the Raman spectra of pentlandite and chalcopyrite from an intergranular aggregate with generally droplike outlines. The main characteristics of these spectra are summarized in Table 3. The peaks of chalcopyrite (349, 317, and 288 cm^{-1}) are slightly shifted compared with those reported in the literature (353, 320, and 293 cm^{-1}) (Mernagh and Trudu, 1993), but there is a generally good agreement. The spectra of both minerals exhibit peaks at 284–288 and 215 cm^{-1}, but their intensities are very different (Table 3). The Raman spectroscopy of pentlandite revealed the dependence of main spectral parameters on the chem-

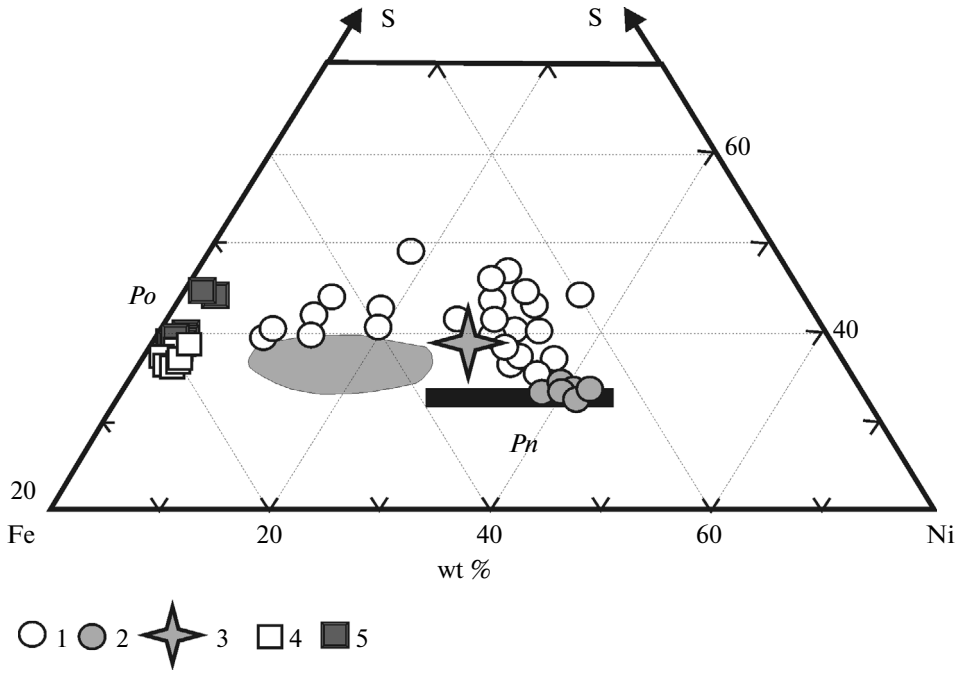

Fig. 3. Compositions of sulfides in the Fe–Ni–S (wt %) system (Kullerud et al., 1969). (1)–(3) Sulfides from the Antarctic xenoliths: (1) inclusions in orthopyroxene and olivine, (2) pentlandite from intergranular aggregate, (3) calculated bulk composition of sulfide melt at 1040–1060°C; (4) and (5) sulfides from inclusions in the xenoliths of Shavaryn-Tsaram, Mongolia: (4) inclusion in the mineral of the druse and (5) inclusion in a clinopyroxene megacryst. The shaded field shows the bulk compositions of sulfides from mantle xenoliths worldwide (Alard et al., 2000). The black band is the field of pentlandite compositions.

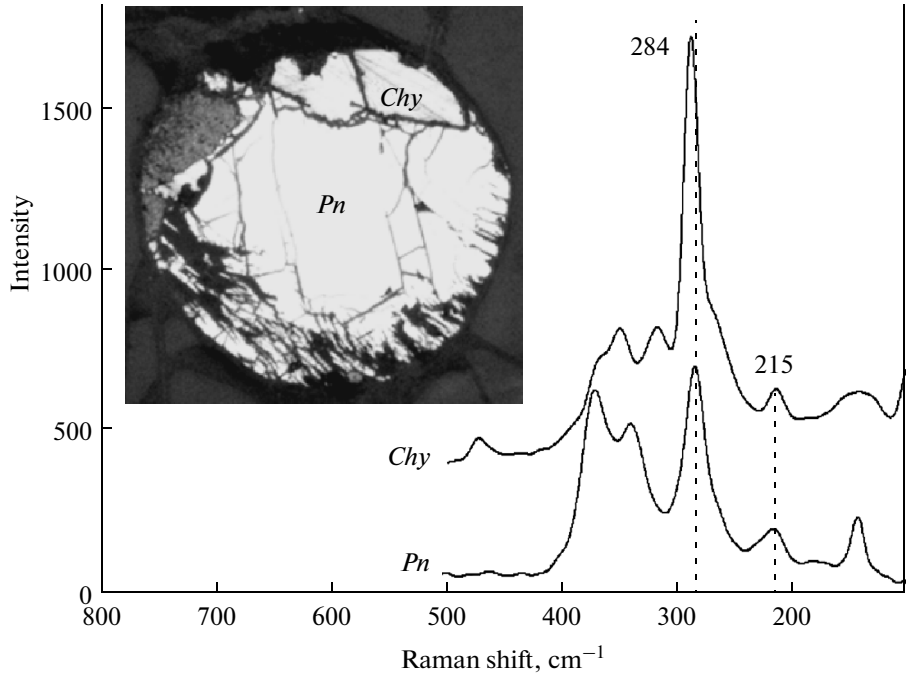

Fig. 4. Raman spectra of chalcopyrite and pentlandite from intergranular aggregates in the East Antarctic xenoliths (one of such aggregates is shown in the inset).

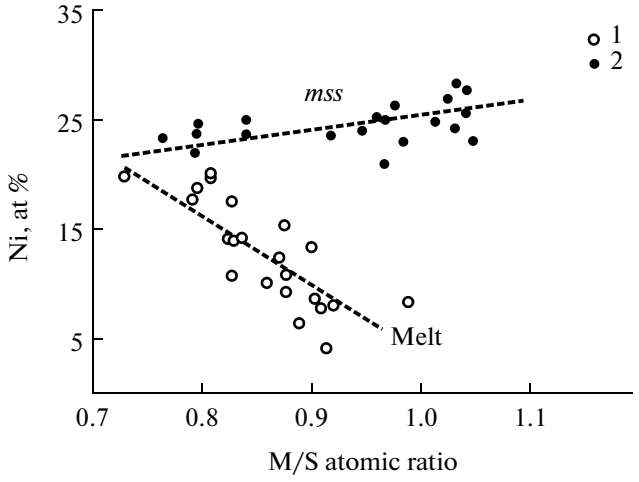

Fig. 5. Covariations of the Ni content in sulfide phases from inclusions and the metal/sulfur ratio (M/S): (1) sulfide melt and (2) monosulfide solid solution.

ical composition of particular zones, including the contents of the minor components Co and Cu.

Sulfide Inclusions in Minerals from Antarctica

Sulfide inclusions from 19 clusters were investigated in the Antarctic xenoliths. Among 32 inclusions (Table 4), 20 consisted of a single phase, and 12 contained two phases (Table 5).

Keeping in mind that the Antarctic xenoliths underwent extensive metasomatic alteration, contain abundant fluid components, and are enriched in trace elements, Se, Te, Sn, Bi, and Pb were analyzed by the EDS method. However, only the Pb content appeared to be above the detection limit and ranged in four analyses from 0.35 to 0.8 at %. It was shown (Hart and Gaetani, 2006) that Pb in mantle peridotites is concentrated mainly in sulfides because of the high partition coefficient of Pb between sulfide and silicate melts. The Bi content approached the detection limit in several analyses (up to 0.28 at %). The presence of Se and Te was established qualitatively.

Multiphase sulfide inclusions in peridotite minerals have been described by many researchers (e.g., Lorand and Grégoire, 2006; Patten et al., 2013). Accessory sulfides in diamonds, eclogites, and kimberlites, as well as inclusions in phenocrysts of igneous rocks of deep origin are perhaps of the same type (Stone et al., 1989; Sharygin et al., 2003).

The analysis of studies on early sulfide occurrences shows that they are almost always represented by crystalline phases, including pyrrhotite, chalcopyrite, and less common pentlandite, violarite ($Fe_xNi_{1-x}Ni_2S_4$), heazlewoodite $(Fe_xNi_{1-x})_{3\pm y}S_2$, and godlevskite $(Fe_xNi_{1-x})_9S_8$ or solid solution on the basis of these phases (Sharygin et al., 2003). Single-phase inclusions are much less abundant (e.g., Alard et al., 2002; Lorand et al., 2004) and were interpreted as a monosulfide solid solution with variable Ni content (*mss*).

None of the aforementioned sulfide phases, except for *mss*, were ever found as inclusions in the minerals of the Antarctic xenolith.

The compositions of sulfide inclusions are shown in the Ni–M/S diagram (Fig. 5), which display two distinct trends with positive and negative correlations. Most of the inclusions are metal-deficient, M/S ≤ 1, which indicates oxidizing conditions during their stabilization (Ballhaus et al., 2001). Foley et al. (2006) estimated that the logarithm of oxygen fugacity relative to the FMQ buffer, f_{O_2} (FMQ), lies between –0.37 and –1.18.

Taking into account the significant differences in the composition of these inclusions, it can be suggested that they are composed of two monosulfide solid solutions (e.g., Fleet and Pan, 1994; Guo et al., 1999; Lorand et al., 2006), two melts (Ballhaus et al., 2001), or melt and *mss* (Li et al., 1996; Ballhaus et al., 2001).

A comparison of experimental results (Naldrett et al., 1997; Ballhaus et al., 2001; Li et al., 1996) obtained at temperatures of 1000–1080°C and M/S = 0.87–0.91 in the starting mixtures with the phases of inclusions observed by us allows us to interpret them as coexisting pentlandite-based *mss* and sulfide melt.

Many authors noted that sulfide melts are poorly quenched in experiments even at rapid cooling (Fleet and Pan, 1994; Kress, 1997; Ballhaus et al., 2001; Mungall and Su, 2005). The products of high-temperature experiments usually show a microscopic heterogeneity, which is also characteristic of the sulfide inclusions examined by us.

In addition to Ni, some sulfide droplets contain Cu. Copper-bearing melts were obtained in experiments at temperatures no higher than ≤950° (Fleet and Pan, 1994). These authors reported the formation of a ternary (Fe, Cu, Ni) sulfide solid solution at temperatures below 850°C. In our inclusions, the Cu content of quenched melt and *mss* is up to 5.9–5.8 at % (Table 4), which implies that they were formed at a later low-temperature stage of the evolution of the sulfide system (Stone et al., 1989).

The analyses of sulfides from two-phase inclusions are given in Table 5. As can be seen in back-scattered electron (BSE) images (Fig. 6a), a partly faceted light gray phase (*mss*) may occupy up to half of the inclusion volume. In the Ni–M/S diagram (Fig. 6b), the compositions plot along the trends of *mss* and sulfide melt.

The coexistence of *mss* and sulfide melt in the inclusions allows us to calculate the Ni partition coefficient between them. The obtained values range from 0.99 to 3.23 (Table 5). The experiments of Ballhaus et al. (2001) revealed a negative correlation between temperature and D_{Ni} *mss*/melt. This dependence can be used to estimate the temperature of quenching of two sulfide phases in the inclusions as 920–1060°C (Fig. 7).

Table 5 presents also the bulk composition of initial sulfide melt calculated for the highest temperature

Table. 4. Composition of single-phase sulfide inclusions in orthopyroxene and olivine, East Antarctica

Component	1*	2	3	4	5	6	7	8
S, wt %	39.74	39.42	41.26	40.24	38.86	42.10	40.84	35.83
Ni	13.86	28.37	25.81	19.40	18.48	31.61	28.36	11.18
Co	0.15	0.88	0.52	0.42	0.00	0.46	0.60	0.00
Fe	46.25	27.71	32.23	39.87	38.35	24.32	22.99	38.61
Cu	0.00	0.00	0.00	0.02	0.34	1.47	1.58	8.14
Total	100.00	96.38	99.82	99.95	96.03	99.96	94.37	93.76
S, at %	53.74	52.79	55.65	54.41	54.03	56.65	52.41	51.60
Ni	10.24	20.74	19.02	14.33	14.03	23.23	19.88	8.79
Co	0.11	0.64	0.38	0.31	0.00	0.34	0.42	0.00
Fe	35.91	21.30	24.96t	30.94	30.61	18.78	16.94	31.92
Cu	0.00	0.00	0.00	0.02	0.24	1.00	1.02	5.91
M/S atomic ratio	0.86	0.81	0.80	0.84	0.83	0.77	0.73	0.90
Phase	melt	melt	melt	melt	melt	melt	melt	melt
Component	9	10	11	12	13	14	15	16
S, wt %	39.85	39.89	37.89	34.88	36.71	35.45	40.83	36.09
Ni	31.81	33.9	24.72	36.17	33.44	32.58	33.29	27.27
Co	0.77	0.43	0.00	0.31	0.27	0.33	0.38	0.56
Fe	27.44	25.68	24.66	27.93	28.54	28.89	18.6	27.07
Cu	0.00	0.00	0.00	0.63	1.04	2.74	6.9	8.18
Total	99.87	99.90	87.27	99.92	100.00	99.99	100.00	99.17
S, at %	54.29	54.36	55.80	49.01	50.96	49.66	55.64	50.76
Ni	23.68	25.23	19.88	27.77	25.36	24.93	24.78	20.94
Co	0.57	0.43	0.00	0.24	0.21	0.25	0.28	0.43
Fe	21.46	20.09	20.85	22.53	22.74	23.23	14.55	21.85
Cu	0.00	0.00	0.00	0.45	0.73	1.93	4.74	5.81
M/S atomic ratio	0.84	0.84	0.73	1.04	0.96	1.01	0.8	0.97
Phase	*mss*	*mss*	*mss*	*mss*	*mss*	*mss*	*mss*	*mss*

Phases: "melt" is quenched sulfide melt, and *mss* is monosulfide solid solution.

* Analysis number.

Table 5. Compositions of coexisting monosulfide solid solution and sulfide melt in six inclusions, at %

Inclusion no.	S	Ni	Co	Fe	Cu	M/S	D_{Ni} *mss*/melt	*T*, °C	Phase
1	49.66	24.93	0.25	23.23	1.93	1.01	0.99	1060	*mss*
	54.36	25.23	0.43	20.09	0.00	0.84			melt
2	49.25	27.10	0.36	22.98	0.00	1.02	1.31	1040	*mss*
	52.79	20.74	0.64	21.30	0.00	0.81			melt
3	50.53	25.20	0.39	21.81	1.45	0.97	1.76	1020	*mss*
	53.81	14.35	0.00	29.78	0.30	0.83			melt
4	50.35	26.32	0.00	22.89	0.00	0.98	2.09	1000	*mss*
	53.45	12.60	0.51	33.44	0.00	0.87			melt
5	48.67	28.47	0.00	21.30	0.34	1.03	2.99	930	*mss*
	52.65	9.52	0.00	36.62	0.06	0.88			melt
6	46.80	25.65	0.00	22.10	0.93	1.04	3.23	920	*mss*
	52.36	7.94	0.00	39.70	0.00	0.91			melt
1–2	51.51	24.50	0.42	21.90	0.48	0.92	–	1060–1040	Bulk

Temperature (*T*, °C) was estimated using the data of Ballhaus et al. (2001). "Bulk" is the composition of initial sulfide melt at 1040–1060°C, "melt" is quenched sulfide melt, and *mss* is monosulfide solid solution.

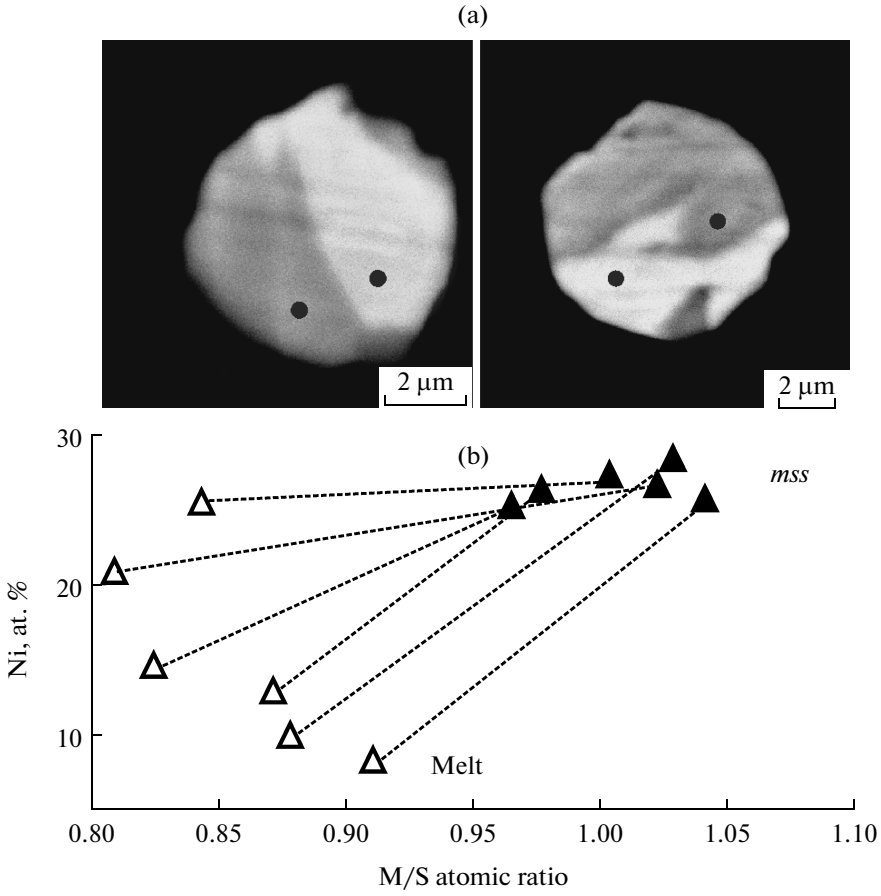

Fig. 6. (a) Back-scattered electron images of two-phase inclusions (dots show the location of analyzed spots). (b) Compositions of coexisting melts and *mss* in the Ni–M/S diagram.

inclusions (1040–1060°C). It is characterized by Ni dominance over Fe (Ni/Fe = 1.12), low Cu content (no more than 0.5 at %), and M/S = 0.92.

A notable feature of the natural two-phase sulfide assemblages in the inclusions is a relatively high S content in the melt compared with *mss* (Fig. 8).

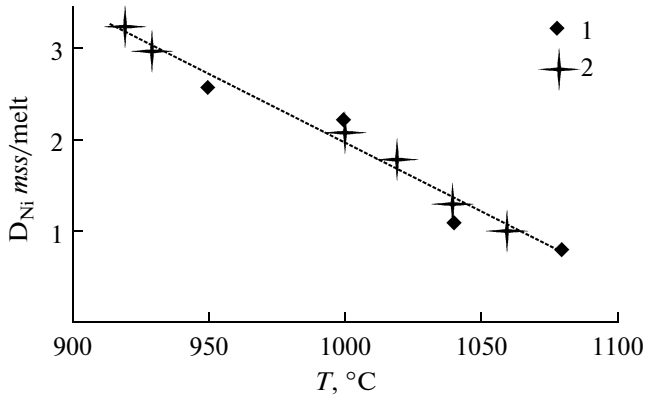

Fig. 7. Dependence of Ni partition coefficient (D_{Ni}) between *mss* and sulfide melt on temperature. (1) Experimental data of Ballhaus et al. (2001) and (2) inclusions described here.

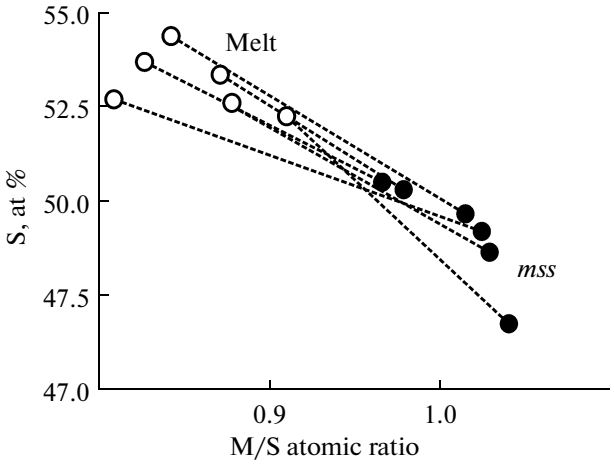

Fig. 8. Sulfur content as a function of the M/S ratio in coexisting sulfide melt and *mss* from inclusions (Table 5).

Table 6. Characteristics of the Raman peaks of monosulfide solid solution and quenched sulfide melt

Analysis no.	*mss*			Melt		
	peak	rel. int.	width	peak	rel. int.	width
1	–	–	–	665.3	90.4	75.7
2	657.5	184.3	98.1	–	–	–
3	370.4	1513.5	144.0	371.6	129.7	48.2
4	–	–	–	342.5	28.6	17.5
5	320.7	35.6	21.2	–	–	–
6	286.3	190.4	21.5	285.2	287.0	49.8
7	216.2	63.3	13.8	215.8	48.8	25.2
8	141.2	88.8	19.5	144.2	51.0	13.5

"Peak" is the position of the peak in the spectrum, cm^{-1}; "rel. int." is the relative intensity of the peak; and "width" is the peak width, cm^{-1}.

Raman Spectroscopy of Inclusions

Since the investigation of the chemical composition of inclusions revealed the presence of several phases, a Raman spectroscopic investigation of the sulfides was undertaken to check this conclusion. Such data are absent in the available literature. The obtained results are shown in Table 6 and Fig. 9.

The differences between the Raman spectra of *mss* and quenched sulfide melt concern mainly the intensity of peaks (Table 6). For instance, the intensity of the 370–371 cm^{-1} peak of *mss* is almost 12 times that of sulfide melt. More significant specific features of the *mss* spectrum is the absence of vibrations at 342 cm^{-1} and the appearance of an additional peak at 320 cm^{-1} (Fig. 9). A pentlandite crystal from an intergranular aggregate contains a droplike inclusion of sulfide melt, whose Raman spectrum is identical to the spectra of orthopyroxene-hosted melt inclusions. Monosulfide solid solution has a more ordered crystal structure and is characterized by stronger atomic vibrations. Thus, the obtained Raman data support our suggestion on the different nature of two Ni-rich sulfide phases in the inclusions.

Secondary Products of Sulfide Alteration (Antarctica)

In addition to sulfides, the intergranular aggregates contain small crystals of magnetite and Cr-rich spinel containing up to 3.83 wt % TiO_2, 4.32 wt % Al_2O_3, 0.8 wt % V_2O_5, and 0.8 wt % MnO. The optical examination of the sample revealed areas at fractures and margins of the aggregates containing alteration products of the primary material. The analysis of these phases showed that some of them have high S contents (up to 57 at %, Table 7). In other areas, there are phases containing only Fe and O with a minor S admixture and oxide totals of up to 88.68 wt %. Sec-

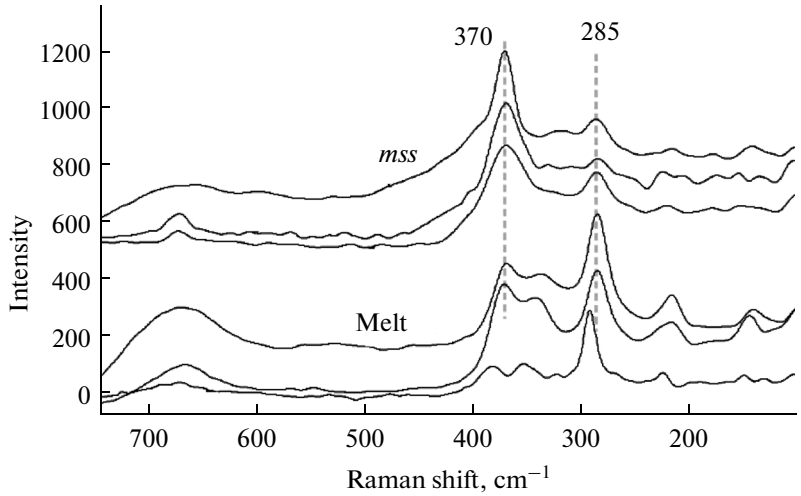

Fig. 9. Raman spectra of quenched sulfide melt and monosulfide solid solution from inclusions.

Table. 7. Compositions of the products of secondary alteration of intergranular sulfide aggregate, East Antarctica

Component	1*	2	3	4
S, wt %	35.06	29.69	41.39	40.99
Ni	45.04	32.63	34.14	38.03
Co	0.04	0.00	0.54	0.64
Fe	11.87	28.47	21.73	19.41
Cu	8.00	9.21	0.00	0.00
S, at %	49.70	43.34	56.85	55.96
Ni	34.88	26.02	25.61	28.36
Co	0.03	0.00	0.40	0.48
Fe	9.67	23.85	17.13	15.21
Cu	5.72	6.79	0.00	0.00
M/S atomic ratio	1.01	1.31	0.76	0.79

1 and 2 are phases of corona structures at the margin of chalcopyrite grains; and 3 and 4 are phases in the zones of late fractures in pentlandite.

* Analysis number.

ondary phases replacing mantle sulfides were described by Lorand (1990), Mitchell and Keays (1981), and Alard et al. (2002). According to their data, the newly formed phases are iron hydroxides and/or goethite, $Fe(OH)_3$. According to these authors, the deficit of analytical totals cannot be assigned to H_2O only. It was conjectured that sulfur could occur as sulfate. The development of secondary hydrous phases (iron hydroxides and goethite) after primary sulfides in the xenoliths could be due to an increase in oxygen fugacity at late stages of magma evolution owing to the dissociation of magmatic water to oxygen and hydrogen (Parodi et al., 1989). The removal of hydrogen and interaction of oxygen and residual water with iron oxides must occur most intensely at temperatures of 750–550°C (Haggerty, 1976). Lorand (1990) noted that iron hydroxides could be formed after sulfides only at temperatures below 500°C.

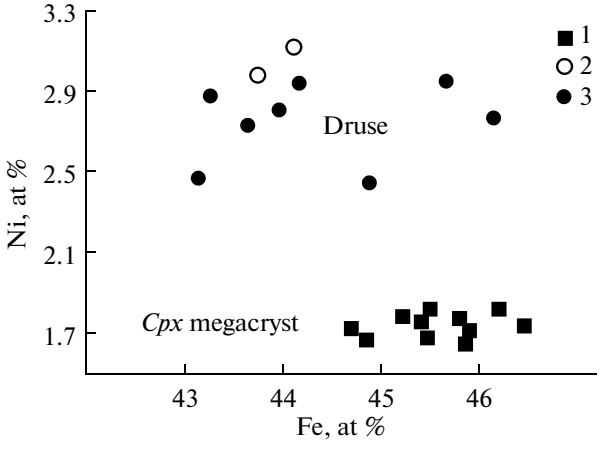

Fig. 10. Fe–Ni (at %) diagram for the compositions of sulfides in (1) clinopyroxene megacrysts and (2) clinopyroxene and (3) garnet from a druse in the peridotites of Mongolia.

Tiny phases (Fig. 1d) enriched in Ni (up to 34.9 at %, Table 7) were often observed at the periphery of chalcopyrite crystals. The occurrence of such crystals only at the boundaries of large chalcopyrite grains with the formation of corona textures allows us to suggest that they are products of late-stage pentlandite–fluid interaction.

Sulfides in the Mongolian Peridotites

In contrast to sulfides from the Antarctic xenoliths, all inclusions in clinopyroxene megacrysts and garnet from the mantle druse of Mongolia are crystalline phases (Table 8), mainly pyrrhotite with a minor Ni content (0.17–3.1 at %). Their Fe/S ratios fall within a narrow range of 0.81–0.89, which corresponds to the sulfide composition Fe_7S_8. Pentlandite was never identified.

In two cases, in a large (up to 50 μm) droplike inclusion in a clinopyroxene megacryst and in a polycrystalline aggregate with a texture suggestive of liquid immiscibility (Fig. 1c), we observed a phase with high Cu content (13.64 and 20.83 at %, respectively) and a Fe/Cu ratio of 2.58 and 1.45, respectively. In both cases, the M/S value approaches 1 (0.98 and 1.06), which allows us to consider this phase as nonstoichiometric chalcopyrite (Vaughan and Craig, 1978), or intermediate solid solution (*iss*) (Fleet and Pan, 1994).

Sulfide inclusions in the minerals of the druse are enriched in Ni compared with those from the clinopyroxene megacrysts (Fig. 10).

The silicate part of the sulfide–silicate–fluid inclusions is 80–90 vol % crystallized and contains clinopyroxene with up to 5 wt % Al_2O_3 and up to 2 wt % TiO_2. Clinopyroxene from the druse is significantly richer in Al_2O_3 (6.86 wt %) and poorer in TiO_2 (1.1 wt %) (Kovalenko et al., 1986). The rim zones of the inclusions contain small patches of glass (melt), and larger portions of residual melts up to a few tens of micrometers across are often observed in the central parts. The aluminosilicate melt is alkali-rich (up to 6.5 wt % Na_2O and 4 wt % K_2O) and contains 51–54 wt % SiO_2, which is illustrated by the maps of the characteristic X-ray emissions of elements (Fig. 11). The mean proportions of silicate, sulfide, and fluid constituents was estimated by counting in many inclusions as 66.5 : 28 : 5.5 (Kovalenko et al., 1986).

Table 8. Compositions of sulfide inclusions in a clinopyroxene megacryst and minerals of the mantle druse, Mongolia

Component	1*	2	3	4	5	6	7	8	9	10	11	12	13	14	15	16
S, wt %	42.73	38.86	38.94	38.09	38.34	38.37	37.68	37.29	37.49	39.35	36.36	38.22	38.35	34.02	38.74	39.13
Ni	2.36	2.01	2.41	2.44	2.32	2.39	2.44	2.33	2.37	2.36	1.82	2.21	1.74	1.98	2.32	2.45
Co	0.30	0.29	0.26	0.28	0.30	0.30	0.30	0.30	0.28	0.33	0.24	0.28	0.30	0.27	0.30	0.34
Fe	51.32	58.51	58.60	57.57	58.76	57.30	58.62	58.57	57.77	57.47	54.74	56.10	57.24	51.96	59.23	57.95
Cu	0.20	0.04	0.03	0.05	0.03	0.03	0.03	0.04	0.68	0.00	0.05	0.00	0.05	0.00	0.03	0.01
S, at %	57.94	52.71	52.58	52.43	52.15	52.74	51.73	51.53	51.75	53.32	52.75	53.24	53.01	52.27	52.23	52.93
Ni	1.75	1.49	1.78	1.83	1.72	1.79	1.83	1.76	1.79	1.74	1.44	1.68	1.31	1.66	1.71	1.81
Co	0.22	0.21	0.19	0.21	0.22	0.22	0.22	0.23	0.21	0.24	0.19	0.22	0.22	0.23	0.22	0.25
Fe	39.95	45.56	45.43	45.49	45.88	45.22	46.20	46.46	45.78	44.70	45.59	44.86	45.42	45.84	45.83	45.00
Cu	0.14	0.03	0.02	0.03	0.02	0.02	0.02	0.03	0.47	0.00	0.04	0.00	0.03	0.00	0.02	0.01
M/S atomic ratio	0.73	0.90	0.90	0.91	0.92	0.90	0.93	0.94	0.93	0.90	0.90	0.90	0.90	0.90	0.91	0.89
Phase	*Po*	*Po*	*Po*	*Po*	*Po*	*Po*	*Po*	*Po*	*Po*	*Po*	*Po*	*Po*	*Po*	*Po*	*Po*	*Po*
Host mineral	*Cpx*	*Cpx*	*Cpx*	*Cpx*	*Cpx*	*Cpx*	*Cpx*	*Cpx*	*Cpx*	*Cpx*	*Cpx*	*Cpx*	*Cpx*	*Cpx*	*Cpx*	*Cpx*
Sample	M-cr	M-cr	M-cr	M-cr	M-cr	M-cr	M-cr	M-cr	M-cr	M-cr	M-cr	M-cr	M-cr	M-cr	M-cr	M-cr
Inclusion type	Sf-Sil-Fl	Sf-Sil-Fl	Sf-Sil-Fl	Sf-Sil-Fl	Sf-Sil-Fl	Sf-Sil-Fl	Sf-Sil-Fl	Sf-Sil-Fl	Sf-Sil-Fl	Sf-Sil-Fl	Sf-Sil-Fl	Sf-Sil-Fl	Sf-Sil-Fl	Sf-Sil-Fl	Drop	Drop

Component	17	18	19	20	21	22	23	24	25	26	27	28	29	30	31
S, wt %	38.95	38.33	31.96	35.31	38.75	39.16	39.29	39.24	39.66	35.74	35.84	37.24	37.59	39.66	38.62
Ni	2.29	2.26	0.20	0.75	4.19	2.37	4.03	3.29	3.71	3.57	3.78	3.61	3.20	3.89	3.96
Co	0.29	0.32	0.11	0.31	0.23	0.25	0.30	0.31	0.32	0.29	0.27	0.33	0.29	0.26	0.33
Fe	58.11	57.79	34.70	42.90	56.57	55.79	56.42	54.71	56.51	56.55	55.67	53.84	56.01	55.72	56.44
Cu	0.00	0.05	27.14	18.95	0.00	1.19	0.00	0.35	0.00	0.05	0.01	0.03	0.03	0.00	0.00
S, at %	52.84	52.55	48.61	50.39	52.62	53.49	53.06	53.91	53.38	50.81	51.19	52.96	52.45	53.66	52.65
Ni	1.70	1.69	0.17	0.58	3.10	1.77	2.97	2.47	2.73	2.77	2.95	2.81	2.44	2.87	2.95
Co	0.21	0.24	0.09	0.24	0.17	0.18	0.22	0.23	0.24	0.22	0.21	0.25	0.22	0.19	0.24
Fe	45.25	45.48	30.30	35.15	44.10	43.74	43.74	43.15	43.66	46.15	45.65	43.96	44.87	43.28	44.17
Cu	0.00	0.03	20.83	13.64	0.00	0.82	0.00	0.24	0.00	0.04	0.01	0.02	0.02	0.00	0.00
M/S atomic ratio	0.89	0.90	1.06	0.98	0.90	0.87	0.88	0.85	0.87	0.97	0.95	0.89	0.91	0.86	0.90
Phase	*Po*	*Po*	*iss*	*iss*	*Po*	*Po*	*Po*	*Po*	*Po*	*Po*	*Po*	*Po*	*Po*	*Po*	*Po*
Host mineral	*Cpx*	*Cpx*	*Cpx*	*Cpx*	*Cpx*	*Cpx*	*Cpx*	*Grt*	*Grt*	*Grt*	*Grt*	*Grt*	*Grt*	*Grt*	*Grt*
Sample	M-cr	M-cr	M-cr	M-cr	Druse	Druse	Druse	Druse	Druse	Druse	Druse	Druse	Druse	Druse	Druse
Inclusion type	Drop	Drop	Sf-Sil-Fl	Drop	Drop	Drop	Drop	Drop	Drop	Drop	Drop	Drop	Drop	Drop	Drop

"M-cr" is the clinopyroxene megacryst; Sf-Sil-Fl is the inclusion of immiscible sulfide and silicate melts with fluid; "Drop" denotes spherical inclusion; *Po* is pyrrhotite; *Grt* is garnet; *Cpx* is clinopyroxene; and *iss* is Fe–Cu intermediate solid solution.

* Analysis number.

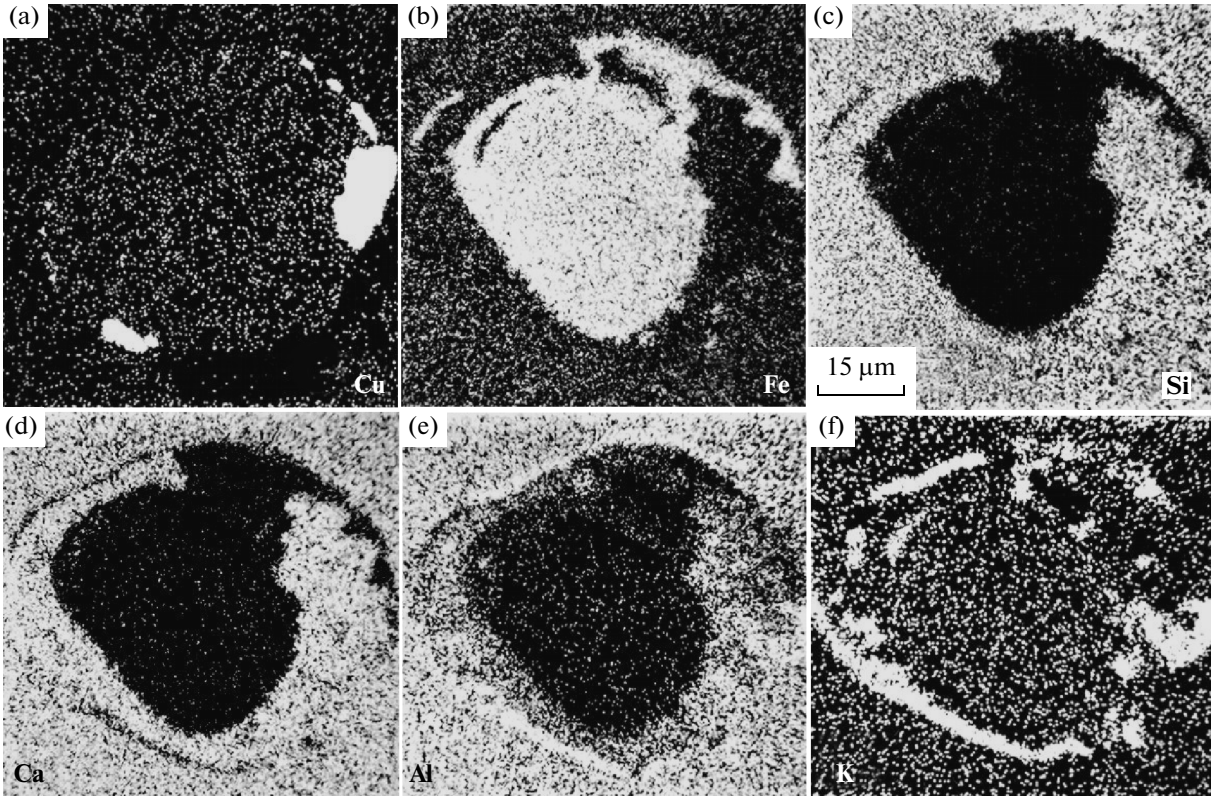

Fig. 11. Elemental X-ray maps of an inclusion in the xenolith of Shavaryn-Tsaram, Mongolia.

INVESTIGATION OF FLUIDS

Composition of Upper Mantle Fluids

The investigation of fluid inclusions in mantle peridotites over many years indicates that carbon dioxide is their dominant component (Kovalenko et al., 1986; Solovova et al., 1990; Rosenbaum et al., 1996; Szabó et al., 2010; Szabó and Bodnar, 1996; Metrich et al., 1999; Andersen and Neumann, 2001; Guilhaumou et al., 2005). The presence of other components of the complex system C–O–H–N–S (N_2, H_2O, CH_4, H_2S, SO_2, CO) has been sporadically reported. There are no experimental data on such a multicomponent system. However, numerous studies addressed simple subsystems of this system, and their results provide a basis for the interpretation of data from fluid inclusions. Since multicomponent fluids were detected in the xenoliths, consider the available literature data on particular components.

Published Data on the Composition of Deep Gases

N_2. Among the above gases accompanying CO_2, nitrogen is the most common fluid component of peridotites and primary magmas derived from the upper mantle and lower crust. Andersen et al. (1995) performed a pioneering study of N_2-bearing fluid inclusions in spinel dunite xenoliths from Lanzarote, Canary Islands. Nitrogen is an important structural impurity in diamonds. Deines et al. (1987) reported up to 750 ppm N, and Taylor et al. (1996) determined up to 1700 ppm N in sulfide-bearing diamond. Fluid inclusions in diamonds may contain up to 40 mol % N_2 (Smith et al., 2015). The experimental investigation of Li and Keppler (2014) showed that, depending on temperature and pressure, nitrogen occurs as NH_3 or N_2 mixed with H_2. The possibility of different nitrogen speciation is intriguing, because NH_4^+ behaves as an equivalent of K^+ in plagioclase, K-feldspar, and mica (Andersen et al., 1993). It was hypothesized that N_2-rich fluids can be produced by oxidation and dehydration reactions related to the destabilization of ammonium-bearing silicate minerals (Dubessy et al., 1989; Andersen et al., 1993). Nitrogen was previously determined by us in melt and fluid inclusions in olivine from the lamproites of Australia (Ryabchikov et al., 1986).

H_2O. Water was very rarely documented in fluids from mantle xenoliths (Trial et al., 1984; Frezzotti and Peccerillo, 2007; Káldos et al., 2011). Based on a revision of published data and their own observations, Frezzotti et al. (1992, 2002, 2012) suggested that the true abundance of H_2O in mantle fluids must be no lower than 10–50 mol %. This hypothesis stemmed from the results of the investigation of fluid inclusions

Table 9. Results of the investigation of primary high-density fluid inclusions from East Antarctica

T_{hom}, °C	T of CO_2 melting, °C	T of phase transitions, °C	Inclusion density, g/cm^3	P at 1050–1080°C, GPa
(–64.0)–(–64.8)	–73.6	(–157)–(–151)	1.17–1.23	>1.1 and up to 2.2

in spinel and garnet peridotites from the Canary Islands, Hawaii, Ethiopian Plateau, and Mediterranean region. Talc, magnesite, chlorides, and sulfates were identified in fluid inclusions from these rocks; the minerals were formed via the reaction of H_2O-bearing fluids with the mineralogical environment. Solovova et al. (2005) described magnesite crystals formed during cooling and decompression in CO_2 fluid inclusions in minerals of olivine melilitites. Berkesi et al. (2012) reported inclusions containing "daughter" magnesite, quartz, Fe sulfide, and films of Fe- and Ca-rich silicate glass. Magnesite and carbon were observed in CO_2 fluid inclusions in olivines from the picritic gabbrodolerite of the Noril'sk complex (Krivolutskaya et al., 2014).

Nonetheless, H_2O retention in fluid inclusions was reported in the literature. For instance, Roedder (1965) showed that olivine from dunite nodules in the Hawaiian basalts contains significant amounts of CO_2 and H_2O, and the CO_2/H_2O mass ratio ranges from 1.6 to 2.33. The Raman spectroscopic investigation of fluid inclusions in peridotitic minerals from the subcontinental lithospheric mantle of Hungary and South Korea at ambient temperature and upon heating up to 150°C and cooling to –100°C revealed the presence of free H_2O molecules and hydroxyl groups (OH^-) (Berkesi et al., 2009; Hidas et al., 2010). Schiano et al. (1995) studied H_2O-bearing fluid inclusions cogenetic with melt inclusions (H_2O content in the glass is up to 5 wt %) in olivine and orthopyroxene from xenoliths of spinel-bearing metasomatized harzburgites from the basaltic andesite lavas of the Philippines island arc. The IR spectroscopy of diamonds from Botswana, Angola, Sierra Leone, and Siberia (Boyd et al., 1992) showed that the main components of fluids are CO_2 and H_2O. The presence of H_2O was also established in fluid inclusions in xenolith from the basalts of Cameroon (Pintér et al., 2011).

Experimental investigations showed that the presence of even minor amounts of H_2O in deep fluids plays an essential role in the extraction and transport of trace and ore-forming elements (Spandler et al., 2014), such as Li, B, LILE, LREE, and U.

H_2S. The presence of trace amounts of H_2S in mantle fluids was established in a few cases by Raman spectroscopy. Metrich et al. (1999) described spinel-bearing harzburgite xenoliths from the basalt lavas of Batan Island with fluid inclusions containing H_2O, sulfide globules, anhydrite, and native sulfur. The authors interpreted such inclusions as an H_2O–S fluid. Hydrogen sulfide was detected in orthopyroxenes and clinopyroxenes of mantle spinel lherzolite xenoliths from the Bakony–Balaton province, Hungary (Berkesi et al., 2009; Hidas et al., 2010) and pyroxenite nodules from Salt Lake Crater, Hawaii (Frezzotti and Peccerillo, 2007). Fluids with H_2S coexisting with pargasite and phlogopite were found in mantle xenoliths from the alkali basalts of the Cameroon Line (Pintér et al., 2011). Gieré (1993) reported interesting results indicating that H_2S-bearing hydrous fluids can transport considerable amounts of Zr, Ti, and REE, up to the crystallization of their own minerals (e.g., zirkelite, $CaZrTi_2O_7$).

SO_2. The presence of SO_2 in fluid inclusions was confirmed by Raman spectroscopy in two cases. In addition to CO_2, gaseous CH_4, N_2, H_2S, and SO_2 were detected in inclusions in olivine and orthopyroxene from spinel lherzolites transported by Hawaiian alkali basalts (De Vivo et al., 1988). Káldos et al. (2011) studied CO_2-rich (94.2 mol %) fluids containing SO_2 (0.1 mol %) and H_2O (5.72 mol %) in spinel lherzolite nodules from South Korea.

CO was identified in CO_2 inclusions from andesine–amphibole veins in xenoliths of amphibole-bearing wehrlites (up to 12 mol %) and metasomatized peridotites (<1 mol %) from Nevada, United States (Bergman and Dubessy, 1984).

Cryometric Investigation of Fluid Inclusions

The cryometric investigation of primary fluid inclusions in minerals from the Antarctic xenoliths revealed their peculiar behavior different from that of pure CO_2 (Table 9). Cooling of single-phase inclusions from ambient temperature to –56.6°C (temperature of coexistence of three phases, gas, liquid, and solid) should have resulted in the appearance of a gas phase in the liquid. However, the inclusions remained homogeneous (liquid) up to –77°C, when the appearance of gas was documented. The temperature of homogenization to liquid (gas dissolution) measured during heating of such multiphase inclusions at a rate of 0.5°C /min was from –64 to –64.8°C. During repeated cooling, a fine-grained aggregate was formed instantaneously at temperatures from –80 to –82.2°C; this aggregate recrystallized within less than one minute into a CO_2 monocrystal, which occupied up to 80% of the inclusion volume. According to the topology of the phase diagram, the melting temperature of CO_2 crys-

tals should be −56.6°C. In our case, this temperature was considerably lower (up to −74.5°C). Moreover, the crystals melted within a certain temperature interval, whereas crystals must melt instantaneously in the pure CO_2 system. For example, in one of the inclusions, the beginning and end of melting were observed at −74.5 and −71°C, respectively. The obtained data provide indirect evidence for the complex composition of fluids in the inclusions. The inclusions were cooled up to −180°C. Because of the small size and faceted shapes of the vacuoles, further optical examination was difficult. Nonetheless, phase transitions were detected unambiguously in the inclusions at temperatures between −151 and −153°C. This temperature is close to the critical temperature of N_2 (−147.1°C), which allows us to suggest that the composition of fluids approaches the CO_2–N_2 system. Its topology (Touret, 1982) indicates that the mole fraction of N_2 in the bulk fluid composition must be approximately 0.20–0.25 at the temperatures of phase transitions observed by us.

According to previous estimates, the minimum melting temperature of CO_2 crystals in CO_2–N_2 fluids must be approximately −62°C (Van den Kerkhof, 1990; Thiery et al., 1994). This is significantly higher than the value measured by us (mean for six inclusions is −73.6). There are two possible explanations for such an anomalous behavior. On the one hand, phase transitions could occur in a metastable field on the continuation of the L + V = S + V equilibrium curve, which was observed previously by many researchers during the thermometric investigation of inclusions (Guilhaumou et al., 1981; Van den Kerkhof and Olsen, 1990). On the other hand, the multicomponent composition of fluid must also affect the temperature of phase transitions during cooling. As will be shown below, the inclusions described here contain additional components mixed with CO_2. In our case, the contributions of both factors were probably significant.

In the pseudosecondary and secondary inclusions, melting of CO_2 crystals was observed at much higher temperatures, from −57.1 to −58.3°C, which are somewhat lower than the melting temperature of pure CO_2 and indicates a *minor* admixture of other volatile components. The behavior of these inclusions was described in more detail by Buikin et al. (2014). The main results of their investigation can be summarized as follows. The highest density of fluids of pseudosecondary inclusions in olivine and clinopyroxene is 0.98 g/cm^3, which corresponds to a pressure of 0.73 GPa. The presence of H_2O in the fluid at an intermediate stage of the evolution of the fluid system is supported by the formation of gas hydrate, which melts at +0.7°C, in some pseudosecondary inclusions. In the secondary three-phase inclusions occurring in healed fractures and containing two liquid phases, CO_2 and H_2O (Fig. 2c), at room temperature, melting of CO_2 crystals was observed at −57.3°C, and the temperature of homogenization to liquid is +15.6°C, which corresponds to a fluid density of 0.83 g/cm^3 and a pressure of up to 0.46 GPa at 950°C.

The compositions of fluid inclusions in minerals of the Mongolian mantle xenoliths and their behavior during cooling are different from those of the Antarctic xenoliths. The melting temperature of CO_2 crystals formed during cooling-stage experiments is −57°C, which indicates the dominance of CO_2 in the fluid composition and a negligible fraction of other gases (Kovalenko et al., 1986). The inclusions are homogenized to liquid at a temperature of up to −31°C, and their density is 1.07 g/cm^3, which corresponds to a pressure of 0.81 GPa. The temperature of formation of the Mongolian mantle druse and megacrysts was estimated using the geothermometer of Wells (1977) as 1100°C. Taking into account that the inclusions were partly opened (decrepitated), the initial pressure at 1100°C could be as high as 1.5 GPa. Similar values of 1.5–1.8 GPa were inferred from the analysis of mineral assemblages (Kovalenko et al., 1985).

Raman Spectroscopy of Fluid Inclusions

Taking into account the unusual behavior of the inclusion during freezing–heating experiments and the problems of the interpretation of obtained thermometric measurements related to the multicomponent composition of the fluids, their composition was constrained using Raman spectroscopy.

It was confirmed that CO_2 is the dominant component of all inclusions (Fig. 12) (Berkesi et al., 2012; Bergman and Dubessy, 1984; Bonelli et al., 2003). In addition, the Raman spectra exhibit peaks of N_2 at 2325–2331 cm^{-1} (Berkesi et al., 2012) and H_2S at 2606–2610 cm^{-1} (Bergman and Dubessy, 1984; Berkesi et al., 2009). The calculation of the ratios of integrated areas of the CO_2, N_2, and H_2S peaks (Dubessy et al., 1989) allowed us to estimate their mole fractions in the fluid of the inclusions as ~0.70 CO_2, 0.15–0.20 N_2, and 0.1 H_2S; the value obtained for N_2 is consistent with the estimate based on cryometric experiments.

The possibility of the existence of fluids with high H_2O contents in the presence of mantle-derived melt is disputable because of the high H_2O solubility in basic and ultrabasic magmas of subalkaline and alkaline series under mantle *P-T* conditions. For instance, glasses from melt inclusions in olivine from the picritic gabbro-dolerites of the Noril'sk complex contain up to 1.3 wt % H_2O, whereas fluid inclusions cogenetic with them are composed of almost pure CO_2 with only traces of H_2O (Krivolutskaya et al., 2001). On the other hand, H_2O is difficult to detect by optical examination if its content is less than 10–20% of the vacuole volume. Nonetheless, freezing-stage observations revealed the formation of gas hydrates in some pseudosecondary inclusions up to 10–15 μm in size, which supports the presence of H_2O in the fluid.

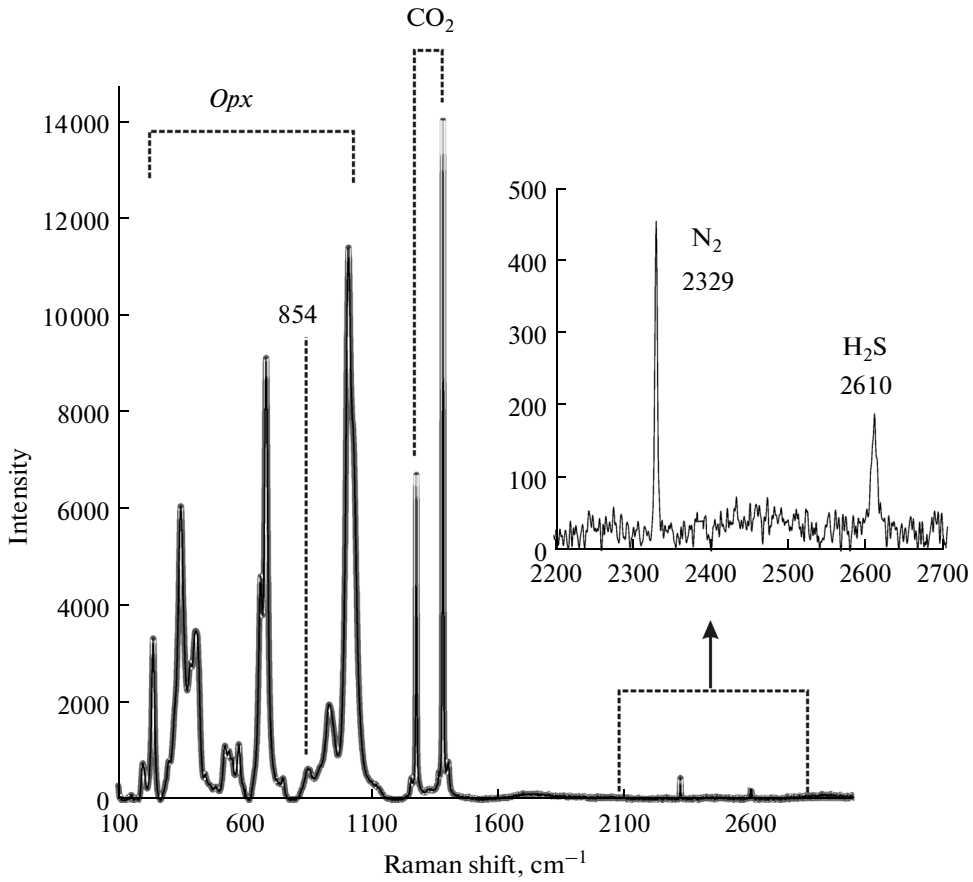

Fig. 12. Raman spectra of fluid inclusions containing CO_2, N_2, and H_2S.

Thus, the composition of the deep fluid corresponds to the multicomponent system C–O–H–N–S. This system includes the compound COS with a characteristic Raman peak at 857 cm^{-1} (Burke, 2001; Giuliania et al., 2003). There is a peak at this position in the obtained Raman spectra. However, the same peak was observed in the spectrum of the host orthopyroxene (Fig. 12). Hence, we cannot definitely conclude that COS occurs in the fluid inclusions.

Some inclusions contain small (no larger than 2 μm) crystals with optical properties of carbonates and a peak at a Raman shift of 1095–1097 cm^{-1} (Frezzotti and Peccerillo, 2007, 2012; Berkesi et al., 2012). Taking into account the carbonate-rich composition of the metasomatic mantle fluid, the phase can be primary. On the other hand, the appearance of carbonate could be due to interaction between CO_2 and the orthopyroxene walls. Such a process was previously observed by us in CO_2 fluid inclusions in the olivine melilitites of Mahlberg, Germany (Fig. 7d in Solovova et al., 2005) and described by Berkesi et al. (2012) and Frezzotti and Peccerillo (2007).

Estimation of Temperature and Pressure

The complex composition of fluids encapsulated in the minerals of the Antarctic xenoliths ($CO_2 > N_2 > H_2S > H_2O$) prevents the accurate determination of its density and, correspondingly, pressure based on freezing-stage measurements. Fortunately, there are other ways of estimating these important characteristics. A CO_2 monocrystal grown repeatedly by the cooling–heating method occupied up to 80% of the inclusion volume. Since the density of solid CO_2 is 1.51 g/cm^3, the density of fluid in the inclusion must be ~1.21 g/cm^3. The maximum temperature was estimated as 1060°C from the partitioning of Ni between coexisting monosulfide solid solution and sulfide melt in six two-phase inclusions. According to Swanenberg (1979, 1980), the pressure of a CO_2–N_2 fluid with an N_2 mole fraction of 0.2 at the estimated temperature and density is 1.1–1.3 GPa.

The Raman spectroscopic data provide independent constraints on CO_2 fluid density. It was shown that the distance between the major CO_2 peaks at 1285 and 1388 cm^{-1} is positively correlated with its density (Yamamoto and Kagi, 2006; Yamamoto et al., 2007).

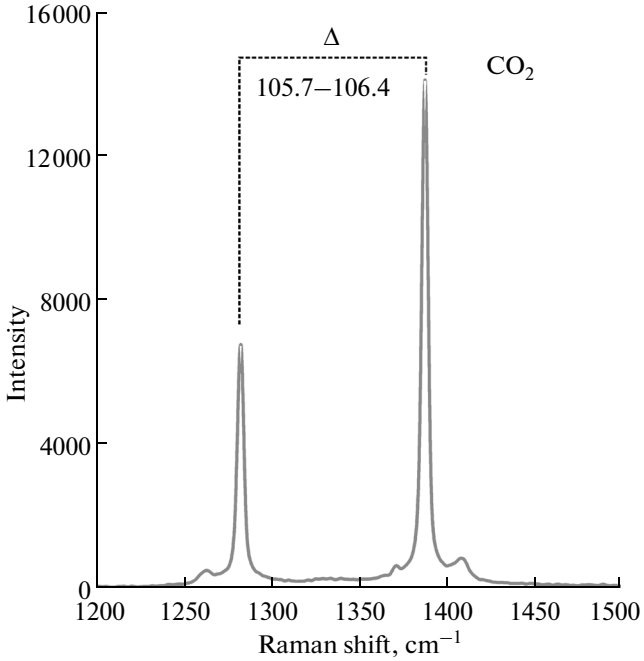

Fig. 13. Position of CO_2 peaks in the Raman spectrum of primary high-density fluid inclusions. The distance between two major CO_2 vibrations (1285 and 1388 cm^{-1}) can be used for the estimation of CO_2 density in the inclusions.

The CO_2 density of the inclusions studied (Fig. 13) ranges from 1.17 to 1.23 g/cm^3. According to Kennedy and Holster (1966) and Pitzer and Sterner (1994), the pressures of CO_2 fluids of such densities must be 1.2–1.5 GPa at 1060°C.

METASOMATIC PROCESSES IN THE MANTLE BENEATH EAST ANTARCTICA

The most important geochemical consequence of the continuous submersion of oceanic crustal material into the mantle is the development of mantle metasomatism, including carbonate metasomatism. One of its large-scale occurrences is the mantle beneath East Antarctic. The detailed investigation of xenoliths from this region (Foley et al., 2006) suggested that active metasomatism was related to one of the last stages of mantle alteration. This conclusion is consistent with the absence of sulfide and fluid inclusions in relics of previously formed mineral assemblages preserved as solid (crystalline) inclusions in the major minerals of rocks in their present state (Buikin et al., 2014).

The presence in the xenoliths of intergranular veinlets of glass with embedded neoblasts of clinopyroxene, olivine, spinel, Ba–Ti-bearing phlogopite, S-bearing chlorapatite, henrymeyerite, calcite, and dolomite (Kogarko et al., 2007) reflects the enrichment of the metasomatizing fluids in trace and rare earth elements (Belyatsky and Andronikov, 2014). Carbonate metasomatism caused the development of calcite and dolomite, CO_2 enrichment, and extensive resorption of clinopyroxene crystals (Buikin et al., 2014). This process can be described by the following reactions:

$$\underset{\text{olivine}}{2Mg_2SiO_4} + \underset{\text{clinopyroxene}}{CaMgSi_2O_6} + \underset{\text{fluid}}{2CO_2} = \underset{\text{orthopyroxene}}{2Mg_2Si_2O_6} + \underset{\text{melt}}{CaMg(CO_3)_2}, \quad (1)$$

$$\underset{\text{melt}}{3CaMg(CO_3)_2} + \underset{\text{clinopyroxene}}{CaMgSi_2O_6} = \underset{\text{calcite}}{4CaCO_3} + \underset{\text{olivine}}{2Mg_2SiO_4} + \underset{\text{fluid}}{CO_2}. \quad (2)$$

The metasomatic character of sulfide mineralization in the mantle materials described here is consistent with the enrichment of the xenolith relative to the composition of the primitive mantle (Palme and O'Neill, 2003) in S (1400 ppm, or seven times that of the primitive mantle), as well as in chalcophile and siderophile elements: Cu (by a factor of 1.5), Ag (by a factor of 83), As (by a factor of 8), Au (by a factor of 2.5), and Ir (by a factor of 1.7) (Table 10). It is known that the equilibrium partition coefficients of chalcophile elements between sulfide and silicate melts are high; for instance, for Ir, it is up to 3×10^4 (Peach et al., 1994).

Table 10. Contents of elements in the mantle and in the garnet–spinel xenolith of East Antarctica

Element	Primitive mantle abundance (Palme and O'Neill, 2003)	Xenolith
Ag, ppb	4	330
As, ppb	66	530
Au, ppb	0.88	2.24
Cu, ppm	20	30
Ir, ppb	3.2	5.5

DISCUSSION

Genesis of High-Pressure Fluid Inclusions

One of the most important problems of interpretation of the obtained data is the genesis of fluid. It was previously shown (Buikin et al., 2014) that the minerals of the garnet–spinel lherzolites contain rare primary and numerous secondary inclusions. The inclusions that have lost part of their material through short fractures not reaching the boundaries of the host mineral were considered as primary (Roedder, 1984). Such a loss happens if the difference between the internal and external pressure reaches a critical value, which depends on the strength of the host mineral and inclu-

Table 11. Composition of Cu-rich sulfide phases from East Antarctica

Component	1*	2	3	4	5	6	7	8	9
S, wt %	35.10	38.83	36.50	40.99	33.49	37.42	39.17	40.26	41.04
Ni	10.95	14.37	21.98	24.14	30.01	33.88	35.65	39.4	42.98
Co	0.00	0.00	0.00	0.26	0.29	0.57	0.19	0.79	0.47
Fe	33.82	26.11	20.03	24.02	26.17	20.95	14.58	15.94	12.98
Cu	18.47	18.34	13.31	10.60	10.32	9.04	9.45	4.41	1.11
S, at %	50.04	53.99	53.51	55.81	47.66	51.39	54.49	54.72	56.38
Ni	8.53	10.91	17.60	17.95	23.32	25.4	27.09	29.24	32.26
Co	0.00	0.00	0.00	0.19	0.23	0.43	0.14	0.58	0.35
Fe	27.68	20.85	16.86	18.77	21.38	16.52	11.65	12.44	10.24
Cu	13.29	12.87	9.85	7.28	7.41	6.26	6.63	3.02	0.77
M/S atomic ratio	0.99	0.83	0.83	0.79	1.10	0.95	0.84	0.83	0.77
Ni/Fe	0.31	0.52	1.04	0.96	1.09	1.54	2.33	2.35	3.15

* Analysis number.

sion size. According to Roedder (1984), small CO_2 inclusions in large olivine crystals survive at a pressure difference of up to 0.7 GPa and a temperature of up to 1200°C; i.e., the initial pressure within the uncracked inclusion could be higher by this value. It is clear that the problem concerns only the high-pressure conditions of formation of deep-seated materials.

With regard to our observations, it should be pointed out that the mantle nature of the densest fluid inclusions was confirmed by the isotope geochemical analysis of gases, the host olivine is up to ~1 cm in size, and the diameter of the primary inclusions is no more than 10–12 μm. Pressures of 1.1–1.5 GPa were estimated for such partly decrepitated inclusions, and the initial pressure could be as high as to 2.2 GPa.

The mantle nature of the primary fluid inclusions is also supported by their coexistence with combined melt–fluid inclusions (Fig. 2b). Pressure estimated for the fluid phase of these inclusions is up to 0.57 GPa; however, it should be kept in mind that, besides partial decrepitation, the pressure decrease could be related to the dissolution of volatile components, especially water, in the melt produced by the partial melting of mantle peridotites at high *P–T* parameters.

The lack of reliable evidence for the presence of a fluid phase in the rocks bearing the xenoliths (Mikhalsky et al., 1998) allows us to exclude fluid influx from the magmas transporting the xenoliths.

The maximum pressure for the secondary fluid inclusions, which always occur along late and often pervasive fractures, was no higher than 0.7 GPa and decreased to almost 0.2 GPa (Buikin et al., 2014). Based on isotopic compositions and element ratios of argon and nitrogen, it was suggested that the appearance of late fluids (and secondary fluid inclusions) could be related to binary mixing in the system mantle–atmosphere or mantle–seawater. Our results are consistent with the conclusions of Belyatsky and Andronikov (2014) derived from correlations between $^{143}Nd/^{144}Nd$ and $^{87}Sr/^{86}Sr$.

Reconstruction of the Initial Stage of the Evolution of Mantle Material

The initial *P-T* conditions of the mantle fluid–sulfide assemblage were further constrained using the following published experimental data: the boundary of the stability of the two-phase assemblage *mss* + sulfide melt (Bockrath et al., 2004; Hart and Gaetani, 2006; Li and Audétat, 2012), the solidus of peridotite–$(0.9CO_2 + 0.1H_2O)$ (Wyllie, 1979), and the isochores of $0.8CO_2 + 0.2N_2$ fluid (Swanenberg, 1980) extrapolated to high temperatures and pressures. The estimated temperature–pressure conditions, 1270–1280°C and ~2.2 GPa, lie close to the spinel–garnet transition (Fig. 14). Since numerous published and our own data indicate that the sulfide material was initially a melt, the temperature of its entrapment at 2.2 GPa must approach 1300°C. A comparison of the whole range of the obtained characteristics with *P–T* estimates from mineral equilibria for the garnet–spinel peridotites of East Antarctica (Foley et al., 2006) showed a good agreement with respect to pressure (1.98–2.37 GPa); however, the temperatures reported by Foley et al. (2006) are no higher than 1180°C an significantly lower than our estimates.

Ni-Rich Sulfide Solid Solution (xss)

The finding of Ni-rich sulfides with high Cu contents in the intergranular aggregates (Table 11) raised the question of their mineralogical identification. Initially, we considered them as Cu-bearing pentlandite. However, the examination of polished sections under a microscope, in back-scattered electron images, and in X-ray emission maps of element distribution indicated the formation of an independent phase. Moreover, experimental studies and natural observations (e.g., Gill, 1975; Schwarzenbach et al., 2014) showed that the solubility of Cu in pentlandite is limited and no higher than 3 wt % even at 600°C. The intergranular phase analyzed by us contains up to 18.5 wt % Cu. It is characterized by a negative correlation between

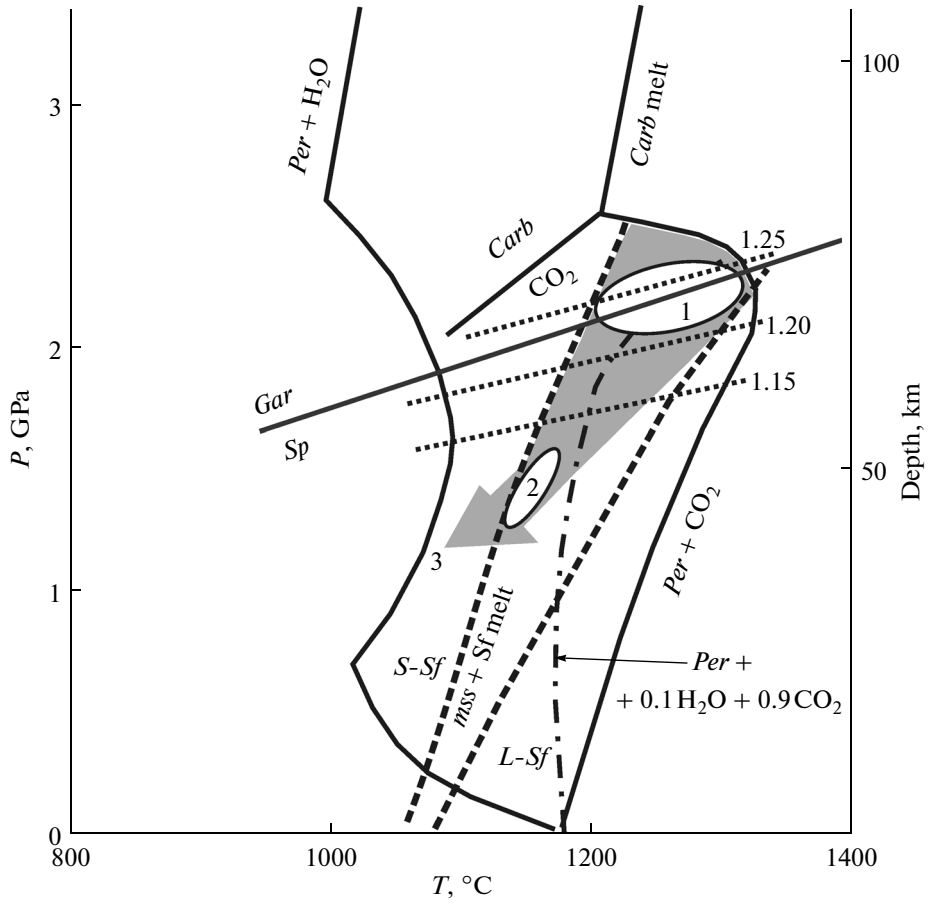

Fig. 14. Evolution of the sulfide–fluid association discussed in this paper in the *P–T* coordinates (Wyllie, 1979). The diagram shows the solidus lines of the peridotite–CO_2, peridotite–H_2O, and peridotite–$(0.1H_2O + 0.9CO_2)$ systems. The field of coexisting monosulfide solid solution and sulfide melt (*mss* + Sf melt) is shown after Bockrath et al. (2004) and Hart and Gaetani (2006). Dotted lines are the isochores of $(0.8CO_2 + 0.2N_2)$ fluid (numbers on the diagram indicate fluid density in g/cm^3) based on the extrapolation of the data of Swanenberg (1979, 1980) to high temperatures and pressures. The gray arrow shows the direction of system evolution. 1 is the area of the fluid-induced metasomatic alteration of mantle peridotites, 2 is the field of temperatures and pressures determined for partly decrepitated inclusions, and 3 is the *P-T* parameters of crystallization of intergranular sulfide aggregates. *L-Sf* and *S-Sf* are the liquidus and solidus of the sulfide system (dash–dot lines).

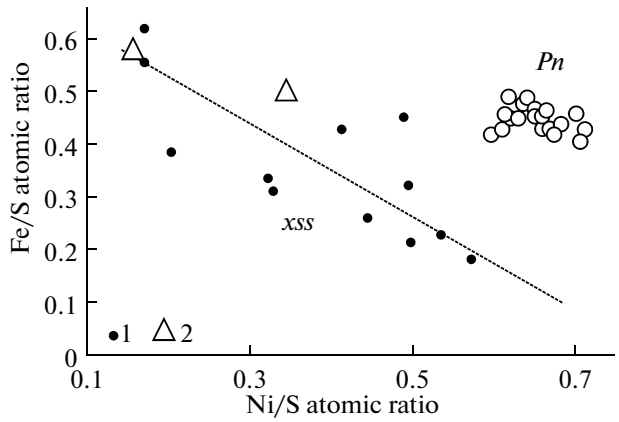

Fig. 15. Variations in the compositions of pentlandite and *xss* in the Fe/S–Ni/S diagram. (1) Our data and (2) products of Fleet and Pan's (1994) experiments.

Ni and Fe (Fig. 15), whereas the pentlandite compositions obtained by us form a separate field at high Ni and Fe contents.

Copper-rich varieties of solid solution and melt (up to 8.1 wt % Cu) were also detected among sulfide inclusions. Fleet and Pan (1994) described two types of intermediate solid solutions in the Fe–Ni–Cu–S system (*iss* and *xss*); one of them (*iss*) contains up to 27 at % Cu and no more than 3.6 at % Ni, and the other (*xss*) referred to as uncharacterized solid solution is richer in Ni (up to 17 at %). It is considered as transitional between *mss* and *iss*, shows relatively high Ni and elevated Cu contents, and is stable at temperatures no higher than 850°C. The minimum temperature estimated for the two-phase sulfide inclusions is 920°C, but the finding of *xss* implies the existence of melt at lower temperatures without textural evidence for *mss* exsolution.

A negative correlation between Cu and the Ni/Fe atomic ratio implies Fe enrichment of the phase during crystallization differentiation (Fig. 16). According to Fleet and Pan (1994) the Ni/Fe value of *xss* ranges from 0.5 to 1.5. The Ni/Fe ratio of the phase from intergranular aggregates varies within 0.3–3.2, and the value observed in the inclusions is 1.49.

Comparison of Mantle Peridotites from Mongolia and Antarctica

Pressure. Our study indicates that the mantle peridotites of Antarctica were affected by hot fluid flows at a pressure no less than 2.2 GPa. Belyatsky and Andronikov (2014) argued that it could be even significantly higher, up to 3.3 GPa; i.e., the processes occurred at depths of up to 100 km.

The established P–T parameters are close to the conditions of carbon occurrence in two forms, as CO_2 fluid and carbonate melt. The finding of sulfide–carbonate intergrowths, the high CO_2 fraction of the multicomponent fluid, and the extensive carbonate metasomatism support our conclusions.

At the Shavaryn-Tsaram complex of alkaline rocks, metasomatic processes occurred at much shallower depths, no greater than 40 km (the maximum pressure was estimated as 1.8 GPa). In the Mongolian peridotites, carbon was found only as CO_2 fluid, whereas crystalline carbonates were never observed.

Temperature. The reconstruction of conditions under which the East Antarctic peridotites were modified indicates much higher temperatures, up to 1300°C, compared with estimates for the mantle rocks of Mongolia (no more than 1100°C).

Composition of fluids. The investigation of mantle peridotite xenoliths from Antarctica and Mongolia showed that they were enriched in fluid components, but the investigation of fluid inclusions revealed considerable differences between them. The fluids of Antarctica have a complex composition and, in addition to CO_2, contain significant amounts of N_2, H_2S, and H_2O. The role of H_2O is supported by the presence of newly formed hydrous phases. The fluids of Shavaryn-Tsaram are almost pure CO_2. They form large pools, inducing the crystallization of unique mantle druses.

Composition of sulfides. Sulfides from the Antarctic xenoliths are enriched in Ni compared with those from the Mongolian peridotites and the average composition of sulfides from mantle peridotites worldwide. Inclusions in the minerals of the Antarctic peridotites contain quenched sulfide melt and monosulfide solid solution in which Ni is more abundant than Fe. The main phase of intergranular aggregates is pentlandite associating with minor chalcopyrite and Ni-rich intermediate solid solution (*xss*). It can be concluded that the mantle beneath East Antarctica is anomalously enriched in Ni, which could be related to the great depth of its formation. This feature, as well as the elevated content of S in the bulk composition of the xenoliths and the presence of an S-bearing component in the fluid, controls the possibility of sulfide melt separation and subsequent precipitation of sulfide minerals.

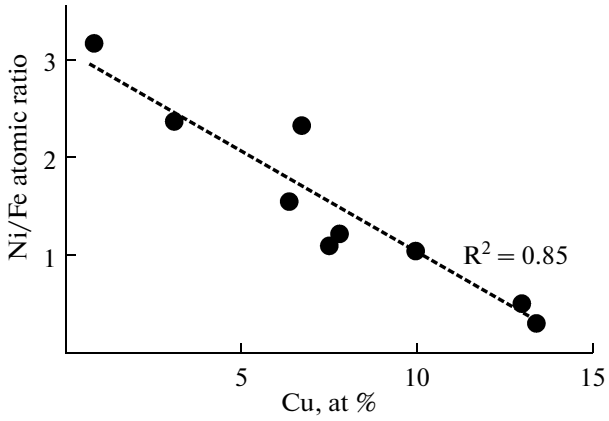

Fig. 16. Correlation of Cu content and the Ni/Fe atomic ratio in intermediate solid solution (*xss*).

In the Mongolian xenoliths, sulfides occur only as inclusions in minerals (clinopyroxene and garnet), whereas intergranular aggregates are absent. The sulfides are represented by pyrrhotite with a minor Ni admixture; i.e., their composition is typical of mantle conditions (Alard et al., 2000). There are only rare findings of chalcopyrite.

ACKNOWLEDGMENTS

The authors thank N.A. Krivolutskaya (Vernadsky Institute of Geochemistry and Analytical Chemistry, Russian Academy of Sciences) for helpful comments and advice and I.G. Griboedova and L.O. Magazina (Institute of Geology of Ore Deposits, Petrography, Mineralogy, and Geochemistry, Russian Academy of Sciences) for high-quality electron microprobe analyses.

This study was financially supported by the Russian Foundation for Basic Research and Russian President's grant.

REFERENCES

Alard, O., Griffin, W.L., Lorand, J.P., Jackson, S.E., and O'Reilly, S.Y., Non-chondritic distribution of the highly siderophile elements in mantle sulfides, *Nature*, 2000, vol. 407, pp. 891–894.

Alard, O., Griffin, W.L., Pearson, N.J., Lorand, J.-P., and O'Reilly, S.Y., New insights into the Re–Os systematics of sub-continental lithospheric mantle from in situ analysis of sulphides, *Earth Planet. Sci. Lett.*, 2002, vol. 203, pp. 651–663.

Andersen, T. and Neumann, E.-R., Fluid inclusions in mantle xenoliths, *Lithos*, 2001, vol. 55, pp. 301–320.

Andersen, T., Austrheim, H., Burke, E.A.J., and Elvevold, S., N_2 and CO_2 in deep crustal fluids: evidence from the Cale-

donides of Norway, *Chem. Geol.*, 1993, vol. 108, pp. 113–132.

Andersen, T., Burke, E.A.J., and Neumann, E.-R., Nitrogen-rich fluid in the upper mantle: fluid inclusions in spinel dunite from Lanzarote, Canary Islands, *Contrib. Mineral. Petrol.*, 1995, vol. 120, pp. 20–28.

Andronikov, A.V. and Mikhalsky, E.V., Deep-seated xenoliths from Proterozoic ultramafic lamprophyre dykes of the Vestfold Hills (East Antarctica): evidence for the existence of metasomatized lithosphere, in *The Antarctic Region: Geological Evolution and Processes*, Ricci C.A., Ed., Siena: University of Siena, 1997, pp. 911–921.

Ballhaus, C., Tredoux, M., and Späth, A., Phase relations in the Fe–Ni–Cu–PGE–S system at magmatic temperature and application to massive sulphide ores of the Sudbury igneous complex, *J. Petrol.*, 2001, vol. 42, no. 10, pp. 1911–1926.

Belyatsky, B.V. and Andronikov, A.V., Age of the upper mantle beneath the Beaver Lake area, East Antarctica: Sm–Nd isotope systematics of mantle xenoliths, *Probl. Arkt. Antarkt.*, 2009, no. 2, pp. 118–138.

Belyatsky, B.V. and Andronikov, A.V., Mantle lherzolite inclusions from alkaline ultrabasic rocks of the Jetty Oasis, East Antarctica: mineralogical–geochemical composition, *P–T* conditions and Sr–Nd isotope characteristics, in *Novoe v geologii i geofizike Arktiki, Antarktiki i Mirovogo okeana* (New in the Geology and Geophysics of Arctica, Antarctica, and World Ocean) St. Petersburg: VNIIOkeangeologiya im. I.S. Gramberga, 2014, pp. 89–109.

Bergman, S.C. and Dubessy, J., CO_2–CO fluid inclusions in a composite peridotite xenolith: implications for upper mantle oxygen fugacity, *Contrib. Mineral. Petrol.*, 1984, vol. 85, pp. 1–13.

Berkesi, M., Hidas, K., Guzmics, T., Dubessy, J., Bodnar, R.J., Szabo, C., Vajnad, B., and Tsunogaee, T., Detection of small amounts of H_2O in CO_2-rich fluid inclusions using Raman spectroscopy, *J. Raman Spectrosc.,* 2009, vol. 40, pp. 1461–1463.

Berkesi, M., Guzmics, T., Szabó, C., Dubessy, J., Bodnar, R., Hidas, K., and Ratter, K., The role of CO_2-rich fluids in trace element transport and metasomatism in the lithospheric mantle beneath the Central Pannonian Basin, Hungary, based on fluid inclusions in mantle xenoliths, *Earth Planet. Sci. Lett.,* 2012, vol. 331–332, pp. 8–20.

Bockrath, C., Ballhaus, C., and Holzheid, A., Fractionation of the platinum-group elements during mantle melting, *Science,* 2004, vol. 305, pp. 1951–1953.

Bonelli, R. and Frezzotti, M.L., Raman Spectra Database. 2003. http://www.dst.unisi.it/geofluids-lab/Raman%20intro.htm

Boyd, S.R., Pillinger, C.T., Milledge, H.J., Mendelssohn, M.J., and Seal, M., C and N isotopic composition and the infrared absorption spectra of coated diamonds: evidence for the regional uniformity of CO_2–H_2O rich fluids in lithospheric mantle, *Earth Planet. Sci. Lett.,* 1992, vol. 109, pp. 633–644.

Brenan, J.M., Se–Te fractionation by sulfide–silicate melt partitioning: implications for the composition of mantle-derived magmas and their melting residues, *Earth Planet. Sci. Lett.,* 2015, vol. 422, pp. 45–57.

Buikin, A.I., Solovova, I.P., Verkhovskii, A.B., Kogarko, L.N., and Averin, A.A., PVT parameters of fluid inclusions and the C, O, N, and Ar isotopic composition in a garnet lherzolite xenolith from the Oasis Jetty, East Antarctica, *Geochem. Int.*, 2014, vol. 52, no. 10, pp. 805–821.

Burke, E.A.J., Raman microspectrometry of fluid inclusions, *Lithos*, 2001, vol. 55, pp. 139–158.

Deines, P., Harris, J.W., and Gurney, J.J., Carbon isotopic composition, nitrogen content and inclusion composition of diamonds from the Roberts Victor kimberlite, South Africa: evidence for ^{13}C depletion in the mantle, *Geochim. Cosmochim. Acta*, 1987, vol. 51, pp. 1227–1243.

De Vivo, B., Frezzotti, M.L., Lima, A., and Trigila, R., Spinel lherzolite nodules from Oahu Island (Hawaii)—a fluid inclusion study, *Bull. Mineralogie*, 1988, vol. 111, nos. 3–4, pp. 307–319.

Dubessy, J., Poty, B., and Ramboz, C., Advances in C–O–H–N–S fluid geochemistry based on micro-Raman spectrometric analysis of fluid inclusions, *Eur. J. Mineral.*, 1989, vol. 1, pp. 517–534.

Farrow, C.E. and Watkinson, D.H., Alteration and the role of fluids in Ni, Cu and platinum-group element deposition, Sudbury igneous complex contact, Onaping-Levack area, Ontario, *Mineral. Petrol.*, 1992, vol. 46, pp. 67–83.

Fleet, M.E. and Pan, Y., Fractional crystallization of anhydrous sulfide liquid in the system Fe–Ni–Cu–S, with application to magmatic sulfide deposits, *Geochim. Cosmochim. Acta,* 1994, vol. 58, no. 16, pp. 3369–3377.

Foley, S.F., Andronikov, A.V., Jacob, D.E., and Melzer, S., Evidence from Antarctic mantle peridotite xenoliths for changes in mineralogy, geochemistry and geothermal gradients beneath a developing rift, *Geochim. Cosmochim. Acta*, 2006, vol. 70, pp. 3096–3120.

Frezzotti, M.L., Burke, E.A.J., De Vivo, B., Stefanini, B., and Villa, I.M., Mantle fluids in pyroxenite nodules from Salt Lake crater (Oahu, Hawaii), *Eur. J. Mineral.*, 1992, vol. 4, no. 5, pp. 1137–1153.

Frezzotti, M.-L. and Peccerillo, A., Diamond-bearing COHS fluids in the mantle beneath Hawaii, *Earth Planet. Sci. Lett.*, 2007, vol. 262, pp. 273–283.

Frezzotti, M.L., Tecce, F., and Casagli, A., Raman spectroscopy for fluid inclusion analysis, *J. Geochem. Explor.*, 2012, vol. 112, pp. 1–20.

Frezzotti, M.L., Touret, J.L.R., and Neumann, E.-R., Ephemeral carbonate melts in the upper mantle: carbonate–silicate immiscibility in microveins and inclusions within spinel peridotite xenoliths, La Gomera, Canary Islands, *Eur. J. Mineral.*, 2002, vol. 14, pp. 891–904.

Gill, J.W., *Pentlandite Phase Relations in the Cu–Fe–Ni–S System,* Montreal: University Montreal, 1975.

Girnis, A.V., Olivine–orthopyroxene–melt equilibrium as a thermobarometer for mantle-derived magmas, *Petrology,* 2003, vol. 11, no. 2, pp. 101–113.

Giuliania, G., Dubessy, J., Banks, D., Vinh, H.Q., Lhomme, T., Pironon, J., Garnier, V., Trinh, P.T., Long, P.V., Ohnenstetter, D., and Schwarz, D., CO_2–H_2S–COS–S_8–AlO(OH)-bearing fluid inclusions in ruby from marble-hosted deposits in Luc Yen area, North Vietnam, *Chem. Geol.*, 2003, vol. 194, pp. 167–185.

Guilhaumou, N., Dhamelincourt, P., Touray, J.C., and Touret, J., Etude des inclusions fluides du systeme N_2–CO_2 de dolomites et de quartz de Tunisie septentrionale, *Geochim. Cosmochim. Acta,* 1981, vol. 45, pp. 657–673.

Guilhaumou, N., Sautter, V., and Dumas, P., Synchrotron FTIR microanalysis of volatiles in melt inclusions and exsolved particles in ultramafic deep-seated garnets, *Chem. Geol.*, 2005, vol. 223, nos. 1–3, pp. 82–92.

Guo, J., Griffin, W.L., and O'Reilly, S.Y., Geochemistry and origin of sulphide minerals in mantle xenoliths: Qilin,

Southeastern China, *J. Petrol.*, 1999, vol. 40, no. 7, pp. 1125–1149.

Haggerty, S., Oxidation of opaque mineral oxides in basalts, *Oxide Minerals*, Rumble D. Ed., *Rev. Mineral.*, 1976, pp. Hl-HI00.

Hart, S.R. and Gaetani, G.A., Mantle Pb paradoxes: the sulfide solution, *Contrib. Mineral. Petrol.*, 2006, vol. 152, pp. 295–308.

Hidas, K., Guzmics, T., Szabo, Cs., Kovacs, I., Bodnar, R.J., Zajacz, Z., Nedli, Zs., Vaccari, L., and Perucchi, A., Coexisting silicate melt inclusions and H_2O-bearing, CO_2-rich fluid inclusions in mantle peridotite xenoliths from the Carpathian–Pannonian region (central Hungary), *Chem. Geol.,* 2010, vol. 274, pp. 1–18.

Káldos, R., Berkesi, M., Hidas, K., Yang, K., and Szabó, Cs., CO_2–SO_2–H_2O fluid inclusions in peridotite xenoliths from Jeju Island (South Korea), *Abst. ECROFI-XXI*, 2011, pp. 112–113.

Kennedy, G.C. and Holster, W.T., Pressure–volume–temperature and phase relations of water and carbon dioxide, in *Handbook of Physical Constants*, Clark S.P., Ed., *Geol. Soc. Amer. Mem.*, 1966, vol. 97, pp. 371–383.

Kogarko, L.N., Kurat, G., and Ntaflos, T., Henrymeyerite in the metasomatized upper mantle of eastern Antarctica, *Can. Mineral.,* 2007, vol. 45, pp. 497–501.

Kovalenko, V.I., Solovova, I.P., Naumov, V.B., Ionov, D.A., and Tsepin, A.I., Mantle mineral formation with participation of carbonic–silicate fluid, *Geokhimiya*, 1986, no. 3, pp. 289–303.

Kovalenko, V.I., Tsepin, A.I., Ionov, D.A., and Ryabchikov, I.D., Garnet–pyroxene druse as an example of fluid crystallization in the mantle, *Dokl. Akad. Nauk SSSR*, 1985, vol. 280, no. 2, pp. 449–453.

Kress, V., Thermochemistry of sulfide liquids I. The system O–S–Fe at 1 bar, *Contrib. Mineral. Petrol.*, 1997, vol. 127, pp. 176–186.

Krivolutskaya, N.A., *Evolyutsiya trappovogo magmatizma i Pt-Cu-Ni rudoobrazovanie v Noril'skom raione* (Evolution of Flood Basalt Magmatism and Pt–Cu–Ni Ore Formation in the Noril'sk District), Moscow: Tovarishchestvo nauchnykh izdanii KMK, 2014.

Krivolutskaya, N.A. and Sobolev, A.V., Magmatic inclusions in olivines from intrusions of the Noril'sk region, northwestern Siberian Platform: evidence for primary melts, *Dokl. Earth Sci.*, 2001, vol. 381A, no. 9, pp. 1047–1052.

Kullerud, G., Yund, R.A., and Moh, G.H., Phase relations in the Cu–Fe–S, Cu–Ni–S, and Fe–Ni–S system, *Econ. Geol.*, 1969, vol. 4, pp. 323–343.

Laiba, A.A., Andronikov, A.V., Egorov, A.V., and Fedorov, L.V., Ultrabasic alkaline stocks and dike bodies at Jetty Peninsula, Prince Charles Mountains, East Antarctica, in *Geological–Geophysical Studies in Antarctica*, Ivanov, V.L. and Grikurov, G.E., Eds., Leningrad: Nedra, 1987, pp. 35–47.

Li, C., Barnes, S.-J., Makovicky, E., Rose-Hansen, J., and Makovicky, M., Partitioning of nickel, copper, iridium, rhenium, platinum, and palladium between monosulphide solid solution and sulphide liquid: effects of composition and temperature, *Geochim. Cosmochim. Acta*, 1996, vol. 60, no. 7, pp. 1231–1238.

Li, Y. and Audétat, A., Partitioning of V, Mn, Co, Ni, Cu, Zn, As, Mo, Ag, Sn, Sb, W, Au, Pb, and Bi between sulfide phases and hydrous basanite melt at upper mantle conditions, *Earth Planet. Sci. Lett.*, 2012, vol. 355–356, pp. 327–340.

Li, Y. and Keppler, H., Nitrogen speciation in mantle and crustal fluids, *Geochim. Cosmochim. Acta*, 2014, vol. 129, pp. 13–32.

Lorand, J.P., Are spinel lherzolite xenoliths representative of the abundance of sulfur in the upper mantle?, *Geochim. Cosmochim. Acta*, 1990, vol. 54, pp. 1487–1492.

Lorand, J.P., Delpech, G., Grégore, M., Moinec, B., O'Reilly, S.Y., and Cottin, J.-Y., Platinum-group elements and the multistage metasomatic history of Kerguelen lithospheric mantle (South Indian Ocean), *Chem. Geol.*, 2004, vol. 208, pp. 195–215.

Lorand, J.P. and Grégoire, M., Petrogenesis of base metal sulphide assemblages of some peridotites from the Kaapvaal craton (South Africa), *Contrib. Mineral. Petrol.*, 2006, vol. 151, pp. 521–538.

Martin, A.P., Cooper, A.F., and Price, R.C., Increased mantle heat flow with on-going rifting of the West Antarctic rift system inferred from characterization of plagioclase peridotite in the shallow Antarctic mantle, *Lithos*, 2014, vol. 190–191, pp. 173–190.

Mernagh, T.P. and Trudu, A.G., A laser Raman microprobe study of some geologically important sulphide minerals, *Chem. Geol.*, 1993, vol. 103, pp. 113–127.

Metrich, N., Schiano, P., Clocchiatti, R., and Maury, R.C., Transfer of sulfur in subduction settings: an example from Batan Island (Luzon volcanic arc, Philippines), *Earth Planet. Sci. Lett.*, 1999, vol. 167, nos. 1–2, pp. 1–14.

Mikhalsky, E.V., Laiba, A.A., and Surina, N.P., The Lambert Province of alkaline-basic and alkaline-ultrabasic rocks in East Antarctica: geochemical and genetic characteristics of igneous complexes, *Petrology*, 1998, vol. 6, pp. 466–479.

Mitchell, R.H. and Keays, R.R., Abundance and distribution of gold, palladium and iridium in some spinel and garnet iberzolites: implications for the nature and origin of precious metal-rich intergranular components in the upper mantle, *Geochim. Cosmochim. Acta*, 1981, vol. 45, pp. 2425–2442.

Morishita, T., Arai, S., and Gervilla, F., High-pressure aluminous mafic rocks from the Ronda peridotite massif, southern Spain: significance of sapphirine- and corundum-bearing mineral assemblages, *Lithos*, 2001, vol. 57, pp. 143–161.

Mungall, J.E. and Su, S., Interfacial tension between magmatic sulfide and silicate liquids: constraints on kinetics of sulfide liquation and sulfide migration through silicate rocks, *Earth Planet. Sci. Lett.*, 2005, vol. 234, pp. 135–140.

Naldrett, A.J., Ebel, D.S., Asif, M., Morrison, G., and Moore, C.M., Fractional crystallisation of sulfide melts as illustrated at Noril'sk and Sudbury, *Eur. J. Mineral.*, 1997, vol. 9, pp. 365–377.

Palme, H. and O'Neill, H., Cosmochemical estimates of mantle composition, *Treatise on Geochemistry*, 2003, vol. 2, pp. 1–35.

Parodi, G.C., Ventura, G.D., and Lorand, J.P., Mineralogy and petrology of an unusual osumilite + vanadium-rich pseudobrookite assemblage in an ejectum from the Vico Volcanic Complex (Latium, Italy), *Am. Mineral.*, 1989, vol. 74, pp. 1278–1284.

Patten, C., Barnes, S.-J., Mathez, E.A., and Jenner, F.E., Partition coefficients of chalcophile elements between sulfide and silicate melts and the early crystallization history of sulfide liquid: LA-ICP-MS analysis of MORB sulfide droplets, *Chem. Geol.*, 2013, vol. 358, pp. 170–188.

Peach, C.L., Mathez, E.A., Keays, R.R., and Reeves, S.J., Experimentally determined sulfide melt–silicate melt par-

tition coefficients for Ir and Pd, *Chem. Geol.*, 1994, vol. 117, pp. 361–377.

Pintér, Zs., Kovács, I., Berkesi, M., Szabó, Cs., Tene Djoukam, J.F., Tchouankoue, J.-P., and Perucchi, A., Unique phlogopite- and amphibole-bearing fluid inclusions in upper mantle xenoliths from Cameroon volcanic line, *Abst. ECROFI-XXI*, 2011, pp. 158–159.

Pitzer, K.S. and Sterner, S.M., Equations of state valid continuously from zero to extreme pressures for H_2O and CO_2, *J. Chem. Phys.*, 1994, vol. 101, pp. 3111–3116.

Roedder, E., Liquid CO_2 inclusions in olivine-bearing nodules and phenocrysts from basalts, *Am. Mineral.*, 1965, vol. 50, pp. 1746–1782.

Roedder, E., *Fluid Inclusions, Rev. Mineral.*, 1984, vol. 12.

Rosenbaum, J.M., Zindler, A., and Rubenstone, J.L., Mantle fluids: evidence from fluid inclusions, *Geochim. Cosmochim. Acta*, 1996, vol. 60, no. 17, pp. 3229–3252.

Ryabchikov, I.D., Mobilization of matter by fluids in the Earth's crust and upper mantle, *Kriterii otlichiya metamorfogennykh i magmatogennykh gidrotermal'nykh mestorozhdenii* (Criteria for Discrimination between Metamorphogenic and Magmatogenic Hydrothermal Deposits), Novosibirsk: Nauka, Sib. Otd., 1985, pp. 64–71.

Ryabchikov, I.D., High NiO content in mantle-derived magmas as evidence for material transfer from the Earth's core, *Dokl. Earth Sci.*, 2003, vol. 389, pp. 437–439.

Ryabchikov, I.D., Solovova, I.P., Sobolev, N.V., Sobolev, A.V., Bogatikov, O.A., Aleshin, V.G., and Vashchenko, A.N., Nitrogen in lamproitic magmas, *Dokl. Akad. Nauk SSSR,* 1986, vol. 288, no. 4, pp. 976–979.

Schiano, P., Clocchiatti, R., Shimizu, N., Maury, R.C., Jochum, K.P., and Hofmann, A.W., Hydrous, silica-rich melts in the sub-arc mantle and their relationship with erupted arc lavas, *Nature*, 1995, vol. 377, no. 6550, pp. 595–600.

Schwarzenbach, E.M., Gazel, E., and Caddick, M.J., Hydrothermal processes in partially serpentinized peridotites from Costa Rica: evidence from native copper and complex sulfide assemblages, *Contrib. Mineral. Petrol.*, 2014, vol. 168, pp. 1–21.

Sharygin, V.V., Pospelova, L.N., Smirnov, S.Z., and Vladykin, N.V., Ni-rich sulfide inclusions in early lamproite minerals, *Geol. Geophys.*, 2003, vol. 44, no. 9, pp. 855–860.

Smith, E.M., Kopylova, M.G., Frezzotti, M.-L., and Afanasiev, V.P., Fluid inclusions in Ebelyakh diamonds: evidence of CO_2 liberation in eclogite and the effect of H_2O on diamond habit, *Lithos*, 2015, vol. 216–217, pp. 106–117.

Solovova, I.P., Naumov, V.B., Kovalenko, V.I., Girnis, A.V., and Guzhova, A.V., Evolution of spinel lherzolite (Dreiser Weiher, Germany): evidence from microinclusion study, *Geokhimiya*, 1990, no. 10, pp. 1400–1411.

Solovova, I.P., Girnis, A.V., Rass, I.T., Kononkova, N.N., and Keller, J., Composition and evolution of fluid-saturated calcium-rich melts: inclusions in the minerals of olivine melilitite from Mahlberg, Rhine Graben, *Geochem. Int.*, 2005, no. 9, pp. 843–861.

Spandler, C., Pettke, Th., and Hermann, J., Experimental study of trace element release during ultrahigh-pressure serpentinite dehydration, *Earth Planet. Sci. Lett.*, 2014, vol. 391, pp. 296–306.

Stone, W.E. and Fleet, M.E., Macrae, N.D., Two-phase nickeliferous monosulfide solid solution (mss) in megacrysts from Mount Shasta, California: a natural laboratory for nickel–copper sulfides, *Am. Mineral.*, 1989, vol. 74, pp. 981–993.

Swanenberg, H.E.C., Phase equilibrium in carbonic systems and their applications to freezing studies of fluid inclusions, *Contrib. Mineral. Petrol.*, 1979, vol. 68, pp. 303–306.

Swanenberg, H.E.C., Fluid inclusions in high-grade metamorphic rocks from S.W. Norway, *Geologica Ultraiectina. Univ. Utrecht*, 1980, no. 25, pp. 1–88.

Szabó, C. and Bodnar, R.J., Changing magma ascent rates in the Nógrád-Gömör volcanic field northern Hungary/southern Slovakia: evidence from CO_2-rich fluid inclusions in metasomatized upper mantle xenoliths, *Petrology*, 1996, vol. 4, no. 3, pp. 221–230.

Szabó, C., Berkesi, M., Hidas, K., Guzmics, T.R.T., Bodnar, R.J., and Dubessy, J., Trace element transport by COHS fluids in the deep lithosphere: a fluid inclusion perspective, *Abst. Goldschmidt Conference*, 2010, p. A1016.

Taylor, W., Canel, D., and Milledge, H.J., Kinetic of Ib to Ia nitrogen aggregation in diamond, *Geochim. Cosmochim. Acta*, 1996, vol. 60, pp. 4725–4733.

Thiery, R., Van den Kerkhof, A.M., and Dubessy, J., νX properties of CH_4–CO_2 and CO_2–N_2 fluid inclusions: modelling for $T < 31^\circ C$ and $P < 400$ bars, *Eur. J. Mineral.*, 1994, vol. 6, pp. 753–771.

Touret, J., An empirical phase diagram for a part the N_2–CO_2 system at low temperature, *Chem. Geol.*, 1982, vol. 37, pp. 49–58.

Trial, A.F., Rudnick, R.L., Ashwal, L.D., Henry, D.J., and Bergman, S.C., Fluid inclusions in mantle xenoliths from Ichinomegata, Japan: evidence for subducted H_2O, *EOS. Transactions of the American Geophysical Union*, 1984, vol. 65, p. 306.

Van den Kerkhof, A.M., Isochoric phase diagrams in the systems CO_2–CH_4 and CO_2–N_2: application to fluid inclusions, *Geochim. Cosmochim. Acta,* 1990, vol. 54, pp. 621–629.

Van den Kerkhof, A.M. and Olsen, S.N., A natural example of superdense CO_2 inclusions: microthermometry and Raman analysis, *Geochim. Cosmochim. Acta*, 1990, vol. 54, pp. 895–901.

Vaughan, D. J. and Craig, J., *Mineral Chemistry of Metal Sulfides*, Cambridge: Cambridge Univ., 1978.

Wells, P.R., Pyroxene thermometry in simple and complex systems, *Contrib. Mineral. Petrol.*, 1977, vol. 62, pp. 129–139.

Wyllie, P.J., Magmas and volatile components, *Am. Mineral.,* 1979, vol. 64, pp. 469–500.

Yamamoto, J. and Kagi, H., Extended micro-Raman densimeter for CO_2 applicable to mantle-originated fluid inclusions, *Chem. Lett.*, 2006, vol. 35, no. 6, pp. 610–611.

Yamamoto, J., Kagi, H., Kawakami, Y., Hirano, N., and Nakamura, M., Paleo-Moho depth determined from the pressure of CO_2 fluid inclusions: Raman spectroscopic barometry of mantle- and crust-derived rocks, *Earth Planet. Sci. Lett.*, 2007, vol. 253, pp. 369–377.

Translated by A. Girnis